MODELLING OF
X-BAND ELECTROMAGNETIC WAVE PROPAGATION

A THESIS SUBMITTED TO
THE GRADUATE SCHOOL OF NATURAL AND APPLIED SCIENCES
OF
MIDDLE EAST TECHNICAL UNIVERSITY

BY

ALİ PELGUR

IN PARTIAL FULFILLMENT OF THE REQUIREMENTS
FOR
THE DEGREE OF MASTER OF SCIENCE
IN
ELECTRICAL AND ELECTRONICS ENGINEERING

AUGUST 2007

Approval of the thesis :

MODELLING OF X-BAND ELECTROMAGNETIC WAVE PROPAGATION

submitted by **ALİ PELGUR** in partial fulfillment of the requirements for the degree of **Master of Science in Electrical and Electronics Engineering Department, Middle East Technical University** by,

Prof. Dr. Canan ÖZGEN
Dean, Graduate School of **Natural and Applied Sciences** _____

Prof. Dr. İsmet ERKMEN
Head of Department, **Electrical and Electronics Engineering** _____

Assoc. Prof. Dr. Sencer KOÇ
Supervisor, **Electrical and Electronics Eng. Dept., METU** _____

Examining Committee Members:

Prof. Dr. Canan TOKER
Electrical and Electronics Eng. Dept., METU _____

Assoc. Prof. Dr. Sencer KOÇ
Electrical and Electronics Eng. Dept., METU _____

Prof. Dr. Gülbin DURAL
Electrical and Electronics Eng. Dept., METU _____

Prof. Dr. Adnan KÖKSAL
Electrical and Electronics Eng. Dept., Hacettepe University _____

Asst. Prof. Dr. Lale ALATAN
Electrical and Electronics Eng. Dept., METU _____

Date: _____

I hereby declare that all information in this document has been obtained and presented in accordance with academic rules and ethical conduct. I also declare that, as required by these rules and conduct, I have fully cited and referenced all material and results that are not original to this work.

Name, Last name :

Signature :

ABSTRACT

MODELLING OF
X-BAND ELECTROMAGNETIC WAVE PROPAGATION

Pelgur, Ali
M. Sc., Department of Electrical and Electronics Engineering
Supervisor : Assoc. Prof. Dr. Sencer KOÇ

August 2007, 86 pages

Calculation of electromagnetic wave propagation over irregular terrain is an important problem in many applications such as coverage calculations for radars or communication links. Many different approaches to this problem may be found in the literature. One of the most commonly used methods to solve electromagnetic boundary value problems is the Method of Moments (MoM). However, especially at high frequencies, the very large number of unknows required in the MoM formulation, limits the applicability of this method, since the memory requirement and the operation count increases by $O(N^2)$ and $O(N^3)$, respectively, where *N* is the number of the unknowns.

Several approaches have been proposed in the literature to reduce the memory requirement and the operation count of the MoM. These approaches rely on the special structure of the impedance matrix generated by the MoM. The Conjugate Gradient (CG) method is a non-stationary iterative technique that can be used to solve general asymmetric/non-Hermitian systems with an operational cost of $O(N^2)$

per iteration. Furthermore, the computational time can be improved by the Fast Fourier Transform (FFT) algorithm to perform the matrix-vector multiplication that appear in any iterative technique. This approach has been successfully used in the literature to solve scattering from electrically large objects and it has been shown that the computational cost and memory requirement can be reduced to O(KNlogN) with K being the number of iterations.

In this thesis, CG method accelerated with Fast Fourier Transform (CG-FFT) method is applied to the problem of electromagnetic propagation over irregular terrain. Applications for electrically large rough terrain profiles are presented. The accuracy of the method is compared to the direct solution of the MoM, CG method and Free Space model with recoveries by Hata model or multiple knife-edge diffraction and reflection. The solution works on quasi-planar surfaces and profiles with small deviation like little breezy sea surface properly.

Keywords: Electromagnetic Wave Propagation, CG-FFT.

ÖZ

X-BANDINDA ELEKTROMANYETİK DALGA YAYILIMININ MODELLENMESİ

Pelgur, Ali
Yüksek Lisans, Elektrik ve Elektronik Mühendisliği Bölümü
Tez Yöneticisi: Doç. Dr. Sencer KOÇ

Ağustos 2007, 86 sayfa

Düzensiz bir arazi üzerinde elektromanyetik dalga yayılımının hesaplanması, radar ve haberleşme linklerinin kapsama alanı belirlenmesi gibi önemli uygulamaları olan bir problemdir. Bu problemin çözümü için literatürde değişik yaklaşımlar önerilmiştir. Elektromanyetik sınır değer problemlerinin çözümünde yaygın olarak kullanılan bir yöntem Method of Moments (MoM) tekniğidir. Ancak, özellikle yüksek frekanslarda MoM formülasyonunun gerektirdiği çok yüksek bilinmeyen sayısı, metodun uygulanabilirliğini sınırlamaktadır. Çünkü, kullanılan bilinmeyen sayısı *N* ise, $O(N^2)$ ile artan hafıza kapasitesi ve $O(N^3)$ ile artan işlem yükü getirmektedir.

MoM yönteminin hafıza gereksinimini ve işlem sayısını azaltmak amacıyla, literatürde değişik yaklaşımlar önerilmiştir. Bu yaklaşımlarda, MoM yönteminde üretilen empedans matrisinin özel yapısı kullanılmaktadır. Eşlenik Eğim (CG) yöntemi, genel asimetrik ve Hermitian olmayan sistemleri, her yinelemede $O(N^2)$'lik işlem sayısı yaparak çözmek için geliştirilen durağan olmayan bir yinelemeli tekniktir. Ayrıca işlem süresi, yinelemeli tekniklerde gerekli olan

matris-vektör çarpımlarının FFT algoritmasıyla gerçekleştirilmesi ile azaltılabilir. Bu yaklaşım, literatürde elektriksel olarak büyük cisimlerden saçılım hesaplarına başarıyla uygulanmış ve hafıza gereksiniminin ve işlem yükünün, K yineleme sayısı olmak üzere, O(KNlogN) değerine indiği gösterilmiştir.

Bu tezde, Fast Fourier Transform yöntemi ile hızlandırılmış CG yöntemi (CG-FFT), düzensiz yüzeyler üzerinde elektromanyetik dalga yayılımı problemine uygulanmaktadır. Elektriksel olarak büyük ve düzensiz yüzey profilleri için örnek uygulamalar sunulmaktadır. Sonuçların doğruluğu MoM matris sisteminin doğrudan çözümü, olağan CG yöntemi ve çeşitli yöntemlerle düzeltilmiş serbest uzay modeli ile karşılaştırılmıştır. Yöntem, düşeyde yüzey değişiminin az olduğu, düze yakın yüzey profillerinde başarılı bir şekilde çalışmıştır.

Anahtar Kelimeler: Elektromanyetik Dalga Yayınımı, CG-FFT.

To Hatice and My Family

ACKNOWLEDGMENTS

The author wishes to express his deepest gratitude to his supervisor Assoc. Prof. Dr. Sencer KOÇ for his guidance, advice, criticism, encouragements and insight throughout the research.

TABLE OF CONTENTS

LIST OF TABLES

LIST OF FIGURES

CHAPTER 1

INTRODUCTION

The enourmous growth in the development of highly reliable, miniature, solid-state radio frequency hardware and the mobile radio communication industry produced the wireless communications era in 1970s. The development powered by digital RF fabrication improvements, VLSI and other technologies made the mobile radio equipment smaller, cheaper and reliable. Since then, people throughout the world have enthusiastically adopted new wireless communication methods and services. The future growth of mobile radio communications will be tied more closely to radio spectrum allocations and regulatory decisions.

The frequency assignment problem has a significant role in sharing well-planned frequency spectrum and obtaining the maximum serviceability. Frequency allocation and planning is a comprehensive study that implies coverage analysis, establishing locations of transmitters or receivers, computation of the interference over the candidate frequencies. Therefore, mobile radio planning requires the accurate computation of electromagnetic field strengths over large areas and in a wide variety of environments. A lot of solution techniques have been developed for this purpose. Some of them are based on propagation prediction models. These are the automatic tools for radio coverage prediction over characteristic geographical databases. Some of the techniques are the integral equation based

methods dealing directly with Maxwell's equations for the computation of scattered field over randomly rough surfaces.

In the numerical solution for x-band propagation over terrain profiles, one has to produce a reliable and fast solution between 9-12 GHz, which is a very useful band for accurate and high data rate signal transmission. Some prediction models can find the empirical solutions be found by

1.1 One-Dimensional (1-D) Rough Surface Scattering Problem

Electromagnetic scattering from rough surfaces has been extensively treated in the literature. A good review can be found in a special issue about this topic, [1]. Most recent advances have been focused on the direct numerical simulation of the scattering problem. Numerical techniques based on integral equation formulations, such as the well-known Method of Moments (MoM), [2], are apparently some of the few sufficiently accurate and robust methods for low-grazing-angle scattering problems.

The primary factor limiting the use of the MoM in the calculation of electromagnetic scattering from rough surfaces is that a linear system of equations must be solved to yield the currents induced on the scatterer. Direct solution methods such as LU decomposition need $O(N^3)$ operations, where N is the number of unknowns in the discretized representation of the surface current. Electrically larger scattering surfaces (for very large N) increase the computational cost and data storing capacity and make these operations prohibitive. This has led to

the development of iterative schemes that solve for the surface current in $O(N^2)$ steps.

1.2 Propagation Prediction Models

Since the computational limitations of integral equation based methods have been due to the large number of surface unknowns, the development of automatic tools for radio coverage prediction over geographical data is a growing interest area. Therefore, the coverage and propagation loss study for wireless communications has become a focus of interest and a great number of propagation models have been developed. According to their nature, the propagation models can be classified as empirical, semi-empirical (or semi-deterministic), and deterministic models.

Empirical models are described by equations or curves derived from statistical analysis of a large number of measured data. Among the empirical methods for predicting the field strength and path loss over terrain profiles for VHF-UHF frequencies, International Telecommunication Union Recommendations, [3-5], and Federal Communications Commission curves, [6], are considered to be the most significant ones. These models are simple and do not require detailed information about the environment. They are also easy and fast to apply because the estimation is usually obtained from experimental measurements. However, they cannot provide a very accurate estimation of the scattered field or the path loss for an arbitrary environment.

Deterministic models are site-specific calculation methods, which physically simulate the propagation of radio waves. Therefore the effect

of the environment on the propagation parameters can be taken into account more accurately than those in the empirical models. Most of the deterministic models are based on ray-optical modelling approaches. The serious disadvantage of ray-optical methods is the computational complexity. Another kind of deterministic methods that have been studied extensively are those derived from the parabolic wave equation (PWE) approximation to the Helmholtz equation, in both integral and differential forms [7-10]. The PWE method is useful in problems where the energy is expected to propagate dominantly in a particular direction. The parabolic wave equation method allows handling the tropospheric refractive index variations, but they neglect the contribution of the backscattered field that is important in some cases and assume only forward propagation. This method is not useful for urban areas and also very undulating profiles.

Semi-deterministic models result from an empirical modification of deterministic models in order to improve the agreement with measurement results. These methods require more detailed information about the environment than the empirical methods but not as much as the deterministic models. Many of them are based on the high frequency asymptotic techniques such as spherical earth diffraction, multiple knife-edge diffraction, geometrical optics and geometrical theory of diffraction. One such model, known as the Spherical Earth Knife Edge, [11], uses a weighted average of analytic solutions for the multi-path, spherical earth, and knife-edge diffraction contributions which depend on the transmitter, receiver and terrain geometries. Another approach is the GTD model described in [12] that is based on the application of the wedge diffraction modified to include finite conductivity and local roughness effects. Both methods have shown reasonable agreement with experimental data but there are

significant differences in some cases that are difficult to explain. Besides, large number of knife-edges or wedges is required to model a terrain profile, which makes their application to real problems very cumbersome.

For the practical application of propagation models there is an important tradeoff between the accuracy of the prediction and the speed with which the prediction can be made.

1.3 Integral Equation Based Methods For Terrain Propagation

Most of the radio propagation prediction methods are obtained by a combination of guesswork and analysis so that they cannot give clear physical picture of the propagation process. So, choosing the best prediction model among a great number of methods becomes an important problem.

Numerical methods, such as integral equation (IE) based methods, become very desirable because they would avoid any kind of uncertainty in the electromagnetic analysis and hence, could be used to check the sensitivity of the true solution to the input terrain data. Besides, they could be used as a reference solution as an alternative to measurements to validate and clarify the limitations of other methods involving approximations. Majority of the integral equation methods are based on the Method of Moments formulation, [2]. The application of the MoM for the electrically large scattering surfaces implies the use of a very large number of surface unknowns, *N*. Therefore, the solution of these kind of problems imply a very high computational cost in terms of CPU time and even terabytes of data storing capacity. In this sense,

the recently developed fast solvers for surface integral equation problems provide an alternative.

The first application of an integral equation method to the terrain propagation problem can be found in [13], where an IE is applied over small terrain profiles. Nevertheless, the application of this method to electrically large terrain profiles becomes impractical, due to the computational cost associated. Later on, in [14], a surface integral equation is derived and simplified with some assumptions such as neglecting back scattering and perfect magnetic conductivity, which make the method more efficient but still very time consuming and less accurate.

As mentioned before, electrically larger scattering surfaces (for very large N) increase the computational cost and data storing capacity and make these operations prohibitive. This has led to the development of iterative schemes that solve for the surface current in $O(N^2)$ steps.

1.4 Iterative Approaches For One Dimensional (1-D) Rough Surface Scattering

For the problem of evaluating the current distribution over a rough surface by means of an iterative method, two different approaches have been followed depending on how the estimates are updated. In the first one, named as stationary technique, the current is updated by applying the surface boundary conditions to the scattered field with the previous iteration's current. Forward – Backward Method (FBM) [15] is a well-known technique. It sweeps the surface on the forward and backward directions to find the forward and backward contributions due to the current element located at a fixed observation point. FBM was

proposed for calculating the electromagnetic current on ocean-like perfectly electric conducting (PEC) surfaces at low grazing angles. The method gives accurate results within very few iterations but the computational cost is still $O(N^2)$. Furthermore, due to its stationary nature, the method fails to converge when the surface of interest is not ordered (reentrant surface of a ship). The second classes of iterative approaches are the non-stationary techniques. These are the extensions of Standard Conjugate Gradient method, [16], that were developed to solve general asymmetric/non-Hermition systems and therefore do not attempt to solve the physical multiple scattering of electromagnetic energy directly. Examples of these are given in [17] where BiConjugate Gradient Method (BiCG) is used. Generalized Conjugate Gradient (GCG) is used in [18], preconditioned multi-grid Generalized Conjugate Residual (GCR) approach is used in [19], and Quasi-Minimum Residual (QMR) is employed in [20].

All of the methods, above, require an operation count of $O(N^2)$. Thus when they are used to solve very-large scale problems, the computational cost and data-storing capacity prohibits their applicability. One has to accelerate the solution to make them applicable. Chou and Johnson, [21], proposed a spectral acceleration (SA) algorithm to overcome the limitation on slightly rough large-scale problems. The algorithm accelerates the matrix-vector multiplications taking place in the iterative process and divides contributions between points in strong and weak regions. The algorithm is mainly based on a spectral representation of two-dimensional Green's function. This technique reduces the computational cost and memory requirements to $O(N)$ and the FBSA (Forward Backward Spectral Acceleration) can be applied over electrically large surfaces. But one should note that the original implementation of spectral acceleration is utilized for slightly

rough quasi-planar surfaces and may not be suitable for undulating rough geometries.

As mentioned previously, the choice of direct methods versus iterative methods is usually made based on the ultimate computational efficiency of the algorithm. Direct methods for dense matrices require $O(N^3)$ operations, while iterative methods require $O(PQ)$ operations, where P is the number of iterations and Q is the operation count per iteration. Electromagnetic problems posed in terms of integral equations with convolutional kernels can sometimes be discretized to yield matrices having discrete-convolutional symmetries and one can solve the scattering problem easily by the circulant or linear discrete convolution, [22,23]. Literature shows that Su, Peters, Volakis, Borup and Gandhi merged conjugate gradient method and fast fourier transform and argued that the fast and the less storing method would be useful in scattering problems, [24,25,26]. For a conjugate gradient with fast Fourier transform (CG-FFT) implementation, where Q may grow as slowly as $N\log N$, an overall computational complexity of $O(PN\log N)$ may be obtained. The CG-FFT approach is attractive when N is large, and the $O(N^3)$ operation count for dense matrices is prohibitive. Unfortunately, the CG-FFT approach is restricted to translationally invariant geometries, which seriously limits its application to practical structures such as urban areas, [25, 27, 28]. An alternative scheme, known as the fast multipole method (FMM), offers the possibility of achieving $O(PN\log N)$ operations for arbitrarily shaped scatterers, [29,30]. Both of the last two methods are competitive for accuracy, solution time and complexity. In the next chapters CG-FFT method, which is the basis of this thesis work, is covered in detail.

This thesis aims to examine CG-FFT over various kinds of terrain profiles to find out if it is preferable in terms of accuracy. In order to achieve these goals, the various implementations of CG-FFT over various kinds of rough surface profiles, are presented.

The conventional CG method with MoM is used as a reference solution with its very accurate solutions and rapid convergence ability, for large numbers of surface unknowns where direct inversion of MoM matrix fails due to the operational and memory cost. Thus, it is applied over some chosen terrain profiles and used as a reference solution in order to examine the CG-FFT results. Of course the reference solutions are limited to a few thousand unknowns. After several numerical experimentation over the CG-FFT, advantages and limitations of the method are detected, and CG-FFT is shown to be useful for the terrain profiles of rough quasi-planar surfaces, and ocean-like surfaces similarly and not to be useful for undulating terrain profiles of urban areas.

CHAPTER 2

SCATTERING PROBLEM FOR 1-D ROUGH SURFACES

2.1 Introduction

This chapter covers the calculation of the current distribution over a surface profile on which an electromagnetic source is incident. The surface considered is assumed to have no variation along the direction transverse to the propagation of the wave. This restriction is necessary to reduce the problem into two dimensions. The variation of the height at the surface along the displacement (*x*-axis) is characterized by the curve *C* and defined by z = f (x) as shown in Figure 2.1 below, yielding the roughness of the surface in one dimension. This surface is illuminated by an incident field {$\boldsymbol{E^i(\rho), H^i(\rho)}$}, where $\rho = x\hat{x} + z\hat{z}$ is the two-dimensional position vector denoting the position along the surface. The terrain profile is modeled to be a non-perfect conductor (with permeability $\mu_r(\rho)$, and permittivity $\in_r(\rho)$ and analyzed using an impedance boundary condition (IBC), [31,32], to be able to investigate more general situations. Assuming the relative permittivity of the scattering surface is large, an approximate IBC can be used. If an IBC is valid, the surface may be treated using a single surface integral equation. Detailed information about IBC can be found in [33-36].This chapter is devoted to the discussion of integral equations in order to find current distribution on the surface of the scatterer. The formulations of integral equations are described in next section.

Corresponding matrix equations to solve these integral equations are determined in last section of this chapter.

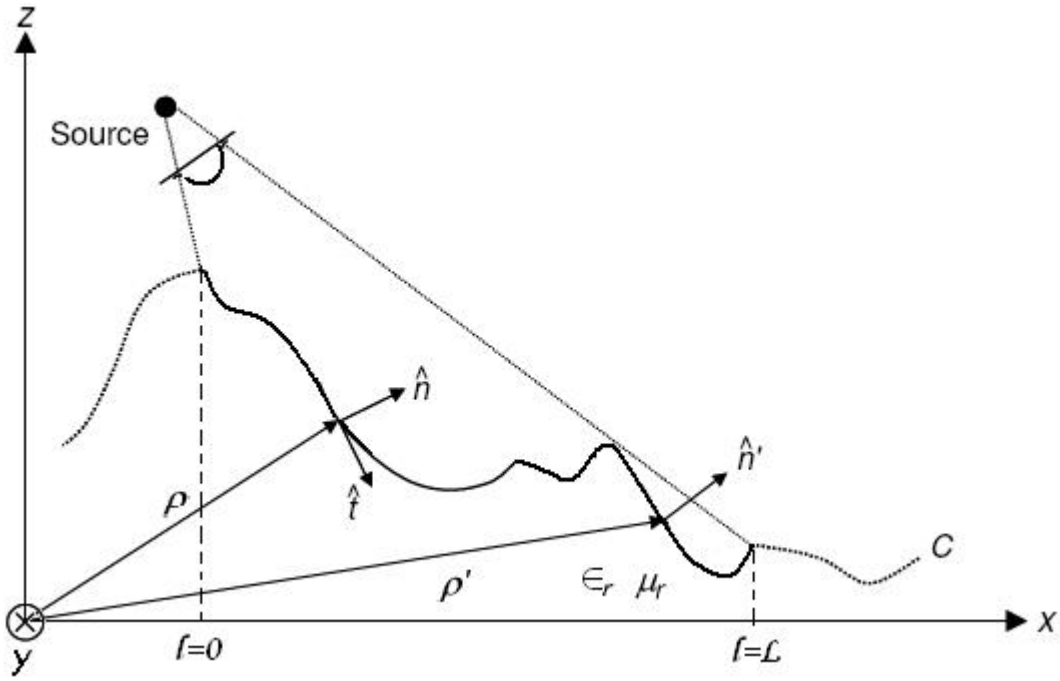

Figure 2.1: A generic terrain profile

2.2 Electric and Magnetic Field Integral Equation Formulations

The solution of a scattering problem is focused on the determination of the physical or equivalent current distribution behavior on the surface of the scatterer. Once they are known, the scattered fields can be evaluated by using conventional radiation integrals. The method used to solve the system should be capable of finding current densities over terrain profiles accurately. This task can be achieved by an integral equation (IE) method.

There are many forms of integral equations. Two of the most popular examples for the time-harmonic electromagnetic fields are known as the Electric Field Integral Equation (EFIE) and the Magnetic Field Integral Equation (MFIE). The EFIE enforces the boundary condition on the tangential electric field and the MFIE enforces the boundary condition on the tangential magnetic field. EFIE will be employed for horizontal polarization; namely, transverse magnetic (TM) case, and MFIE will be utilized for vertical polarization, namely, transverse electric (TE) case. In each case an IBC approximation will be used. The IBC implies that only the electric and magnetic fields external to the scatterer are relevant and their relationship is a function of the material constitution (i.e., surface impedance) or surface characteristics (i.e., roughness) of the scatterer, [37].

An equivalent exterior problem for the rough terrain profile illustrated in Figure 2.1 can be obtained using electric and magnetic sources **J** and **K**, respectively, defined on the surface according to

$$\mathbf{J} = \hat{n} \times \mathbf{H} \tag{2.1}$$

$$\mathbf{K} = \mathbf{E} \times \hat{n} \tag{2.2}$$

and radiating in an infinite space with the same parameters as the exterior medium. Since the relative permittivity is large, the equivalent sources of (2.1) and (2.2) can satisfy the IBC, [34].

$$\mathbf{K}(\rho) = \eta_s(\rho)\mathbf{J}(\rho) \times \hat{n}(\rho) \tag{2.3}$$

Where $\hat{n}$ is the unit normal vector to the surface and η_s is the surface impedance which may vary along the surface. Integral equations for the problem can be formulated to relate the incident electric or magnetic fields to the equivalent sources.

To examine the scattering problem for a general wave polarization, it is most suitable to decompose the electric field into its perpendicular and parallel components relative to the plane of incidence, and analyze each one of them individually, [38]. The total field will be the vector sum of these two polarizations. The transverse magnetic (TM) case, in which the electric field is perpendicular to the plane of incidence, is defined as the horizontal polarization case; while the transverse electric (TE) case, in which the electric field is parallel to the plane of incidence, is called as the vertical polarization case, [27]. Both horizontal and vertical polarization cases are covered in the following subsections.

2.2.1 Electric Field Integral Equation (EFIE) Formulation for Horizontally Polarized Incidence on Non-PEC Surfaces

The unknown current induced on the surface has to be found for a given incident field, which may be radiated by any kind of source, so that the scattered field can be computed. If the incident field on the scattering surface in Figure 2.1 is horizontally polarized, namely, "$\mathbf{E}^{\text{inc}} = \hat{y}E^{\text{inc}}$" and if an impedance boundary condition is valid, then equivalent sources have components J_y and $\mathbf{K}_t$ where "$\hat{t} = \hat{y} \times \hat{n}$" is the unit tangent vector along the surface and on xz-plane, and the IBC reduces to

$$\mathbf{K}_{\text{t}}(\rho) = E_{\text{y}}(\rho)\hat{t} = \eta_{\text{s}}(\rho)H_{\text{t}}(\rho)\hat{t} = \eta_{\text{s}}(\rho)J_{\text{y}}(\rho)\hat{t}\,. \tag{2.4}$$

Since $\hat{t}$ is the unit tangent vector, $\mathbf{K}_{\text{t}}$ denotes the tangential component of the equivalent magnetic source. Then an electric field boundary condition given by

$$E_{\mathbf{y}}^{\,scat}(\rho) + E_{\mathbf{y}}^{\,inc}(\rho) = \eta_s(\rho)J_y(\rho) \tag{2.5}$$

is valid on the scattering surface where $E_{\mathbf{y}}^{inc}$ denotes the incident field and E_y^{scat} denotes scattered field above the scatterer. The electric field integral equation (EFIE) can be written entirely in terms of the equivalent electric current density J_y on the surface as

$$-E_y^{inc}(\rho) = -\eta_s(\rho)J_y(\rho) - j\omega A_y - \frac{1}{\in}\left\{\frac{\partial F_x}{\partial z} - \frac{\partial F_z}{\partial x}\right\} \tag{2.6}$$

where A_y and F_t are the appropriate components of the magnetic and electric vector potentials, respectively, and can be expressed as

$$A_y(\rho) = \mu\int_C J_y(\rho')G(\rho,\rho')d\rho' \tag{2.7}$$

$$\mathbf{F}_t(\rho) = \in\int_C \hat{t}(\rho')\eta_s(\rho')J_y(\rho')G(\rho,\rho')d\rho' \tag{2.8}$$

where μ and $\in$ are the permeability and permittivity of the medium above the rough surface, respectively, [27]. F_t denotes the tangential component of the electric vector potential, and G is the two-dimensional Green's function expressed as,

$$G(\rho,\rho') = \frac{1}{4j}H_0^{(2)}(kR) \tag{2.9}$$

where $H_0^{(2)}$ is the Hankel function of the second-kind with order zero and

$$R = \sqrt{[x(\rho)-x(\rho')]^2 + [z(\rho)-z(\rho')]^2} \tag{2.10}$$

Here, primed coordinates denote the source locations, while unprimed coordinates represent observation points on the surface.

Substituting (2.7) and (2.8) into (2.6), the electric field integral equation can be rewritten as

$$-E_y^{inc}(\rho) = -\eta_s(\rho)J_y(\rho) - j\omega\mu\int_C J_y(\rho')G(\rho,\rho')d\rho' + \int_C \eta_s(\rho')J_y(\rho')\frac{\partial}{\partial n'}G(\rho,\rho')d\rho' \quad (2.11)$$

where, J_y is the surface electrical current on C and $\partial G/\partial n'$ is the derivative of the two-dimensional Green's function with respect to $\hat{n}'$, the normal vector to the surface at the source point ρ', [38].

Assuming that the incident field is finite, the surface and the integration in (2.11) can be confined to a finite region, though the profile C is arbitrarily extended to infinity. Therefore, (2.11) can be solved using a Method of Moments (MoM) discretization process, [2].

The Method of Moments Solution

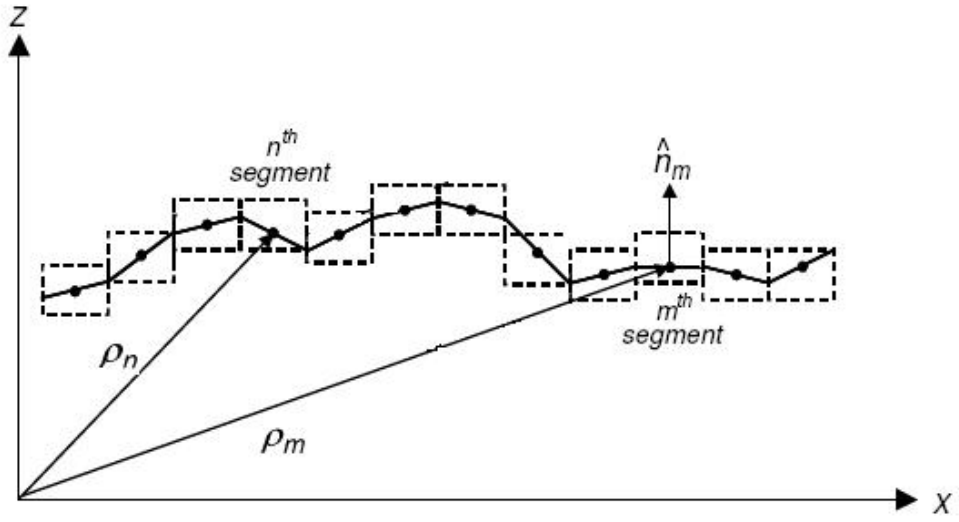

Figure 2.2: Surface discretization

It is necessary to solve (2.11) for the unknown $J_y(\rho')$ and that is an operator inversion problem. (2.11) is an integral equation that can be used to find the unknown induced current $J_y(\rho')$ based on the incident electric field $-E_y^{inc}(\rho)$. The solution may be reached numerically by reducing (2.11) to a series of linear algebraic equations that may be solved by customary matrix equation techniques. To facilitate this, the unknown current density $J_y(\rho')$ is approximated by an expansion in terms of *N* known functions with constant, but unknown coefficients:

$$J_y(\rho') \cong \sum_{m=1}^{N} I_m p_m(\rho') \tag{2.12}$$

The $p_m(\rho')$ functions in the expansion (2.12) are chosen for their ability to accurately model the unknown quantity, while minimizing computation. They are often referred to as *basis* or expansion functions. To avoid the computational cost, subdomain piecewise constant or *pulse* functions will be used. These functions are defined to be of a constant value over one segment and zero elsewhere, such that

$$p_m(\rho') = \begin{cases} 1, & \text{if } \rho' \in \text{segment } m \\ 0, & \text{otherwise} \end{cases} \tag{2.13}$$

The surface is now divided into *N* segments as illustrated in Figure 2.2. Substituting (2.12) into (2.11) and evaluating (2.11) at a fixed observation point on the surface such as p_n, produces an integrand that is solely a function of ρ'. Obviously this leads to one equation with *N* unknowns I_m. In order to obtain a solution for these *N* amplitude constants, *N* linearly independent equations are necessary. Choosing an observation point p_n on the surface at the center of each segment may produce. It is shown in Figure 2.2 (n =1, 2, …, N). This will result in one equation corresponding to each observation point. Since the

integral in (2.11) is nonsingular, interchanging the integration and summation,

$$-E_y^{inc}(\rho_n) \cong -\eta_s(\rho_n) I_n - j\omega\mu \sum_{m=1}^{N} I_m \int_{\Delta x_m} G(\rho_n, \rho_m) d\rho_m + \sum_{m=1}^{N} I_m \int_{\Delta x_m} \eta_s(\rho_m) \frac{\partial}{\partial n_m} G(\rho_n, \rho_m) d\rho_m \tag{2.14}$$

is valid for N such points of observation. The $N \times N$ system produced by (2.14) can be written more concisely using matrix notation as

$$-\begin{bmatrix} E_y^{inc}(\rho_1) \\ E_y^{inc}(\rho_2) \\ \vdots \\ E_y^{inc}(\rho_N) \end{bmatrix} = \begin{bmatrix} Z_{11} & Z_{12} & \cdots & Z_{1N} \\ Z_{21} & Z_{22} & \cdots & Z_{2N} \\ \vdots & \vdots & \ddots & \vdots \\ Z_{N1} & Z_{N2} & \cdots & Z_{NN} \end{bmatrix} \begin{bmatrix} I_1 \\ I_2 \\ \vdots \\ I_N \end{bmatrix} \tag{2.15}$$

or

$$[V_n] = [Z_{nm}] \cdot [I_m] \tag{2.16}$$

In summary, the solution of (2.11) for the current distribution on a rough surface has been accomplished by approximating the unknown with pulse basis functions, dividing the surface into segments, and then sequentially enforcing (2.11) at the center of each segment to form a set of linear equations. The procedure that is followed to convert the continuous integral equation to a discrete matrix equation is a special case of a general approach known as *Method of Moments*. In this special case the basis functions are pulse functions and weighting (testing) functions are impulses. This is also called the *point matching* with *pulse basis functions*, [2].

The entries of the $N \times N$ matrix in (2.15) represent the self and mutual impedances between different segments in the model; thus, this matrix

is called as *the moment method impedance matrix*. The entries of the impedance matrix in (2.15) are given by,

$$Z_{nm} = \int_{\Delta x_m} \left[-j\omega\mu\, G(\rho_n, \rho_m) + \eta_m \frac{\partial}{\partial n_m} G(\rho_n, \rho_m) \right] d\rho_m \qquad (2.17)$$

where ρ_n denotes the observation point which is considered to be located on the center of the n^{th} segment, while ρ_m represents the source point on the center of the m^{th}. If the segments are small compared to the wavelength, typically $\lambda/10$, the elements of the impedance matrix may be approximated as,

$$\begin{aligned} Z_{nm} \cong & -\frac{\omega\mu}{4} \Delta x_m H_0^{(2)}\left(k|\rho_n - \rho_m|\right) \\ & - j\frac{k\eta_m}{4} \Delta x_m H_1^{(2)}\left(k|\rho_n - \rho_m|\right) \hat{n}_m \cdot \hat{\rho}_{nm} \end{aligned} \qquad (2.18)$$

where $H_1^{(2)}$ is the Hankel function of the second-kind with order one, arising from the partial derivative of the Green's function and Δx_m is the length of the m^{th} segment. Also, $\hat{\rho}_{nm}$ denotes a unit vector in the direction from source ρ_m to the receiving element ρ_n, and $\hat{n}_m$ represents the unit normal vector of the surface at ρ_m.

Since the Hankel function is singular for $\rho_n = \rho_m$, the diagonal elements of the impedance matrix cannot be evaluated using (2.18). Moreover, accurate evaluation of the diagonal terms is very important, since they give greater contribution to the solution of the system because of their relatively larger amplitudes. Therefore, the impedance matrix is diagonally dominant, and using the small argument series expansion of the Hankel functions, diagonal entries of the impedance matrix can be obtained as, [27,39],

$$Z_{mm} \cong -\frac{\omega\mu}{4}\Delta x_m\left[1 - j\frac{2}{\pi}ln\left(\frac{\gamma k\Delta x_m}{4e}\right)\right] - \frac{\eta_m}{2} \qquad (2.19)$$

where γ is the Euler constant 1.781072418 and e = 2.718281828.

Note that, the expressions for the PEC case can be deduced by a simple manner through replacing η_m by 0. For the sake of completeness, the expressions for the PEC case are rewritten as follows:

$$Z_{nm} \cong -\frac{\omega\mu}{4}\Delta x_m H_0^{(2)}\left(k\left|\rho_n - \rho_m\right|\right) \qquad (2.20)$$

$$Z_{mm} \cong -\frac{\omega\mu}{4}\Delta x_m\left[1 - j\frac{2}{\pi}ln\left(\frac{\gamma k\Delta x_m}{4e}\right)\right] \qquad (2.21)$$

(2.11) is discretized to form the matrix equation (2.15). The elements of the impedance matrix are obtained in (2.18) and (2.19) for mutual and self-coupling terms, respectively. The system $\mathbf{V} = \overline{\mathbf{Z}} \cdot \mathbf{I}$ should be solved for unknown current coefficients, $\mathbf{I} = \{I_m\}$, [27].

2.2.2 Magnetic Field Integral Equation (MFIE) Formulation for Vertically Polarized Incidence on Non-PEC Surfaces

If the incident field on the scattering surface in Figure 2.1 is vertically polarized, namely, "$\mathbf{H}^{\text{inc}} = \hat{y}H^{inc}$" and if an impedance boundary condition is valid along the surface, then equivalent sources have components $\mathbf{J}_t$ and K_y where "$\hat{t} = \hat{y} \times \hat{n}$" is the unit tangent vector along the surface and on xz-plane, and the boundary condition reduces to

$$K_y(\rho) = -E_t(\rho) = \eta_s(\rho)H_y(\rho) = -\eta_s(\rho)\mathbf{J}_t(\rho) \qquad (2.22)$$

Although the MFIE formulation is generally used for closed surfaces; since the surface is assumed to be arbitrarily extended to infinity, a

magnetic field integral equation can be used to model the vertical polarization problem, [27,38]. Thus, the magnetic field boundary condition

$$H_y^{scat}(\rho) + H_y^{inc}(\rho) = -\mathbf{J}_t(\rho) \tag{2.23}$$

is valid on the scattering surface.

In terms of the tangential induced current J_t, the magnetic field integral equation can be expressed on the surface as

$$-H_y^{inc}(\rho) = \mathbf{J}_t(\rho) - j\omega F_y - \frac{1}{\mu}\left\{\frac{\partial A_z}{\partial x} - \frac{\partial A_x}{\partial z}\right\} \tag{2.24}$$

where **A** and **F** are the magnetic and electric vector potentials, respectively, and their relevant components can be expressed as

$$\mathbf{A}_t(\rho) = \mu \int_C \hat{t}(\rho')\mathbf{J}_t(\rho')G(\rho,\rho')d\rho' \tag{2.25}$$

$$F_y(\rho) = -\in \int_C \eta_s(\rho')\mathbf{J}_t(\rho')G(\rho,\rho')d\rho' \tag{2.26}$$

Substituting (2.25) and (2.26) into (2.24), the magnetic field integral equation can be rewritten as

$$\begin{aligned} -H_y^{inc}(\rho) = \mathbf{J}_t(\rho) + j\omega \in \int_C \eta_s(\rho')\mathbf{J}_t(\rho')G(\rho,\rho')d\rho' \\ -\int_C \mathbf{J}_t(\rho')\frac{\partial}{\partial n'}G(\rho,\rho')d\rho' \end{aligned} \tag{2.27}$$

where, $\partial G/\partial n'$ is the derivative of the two-dimensional Green's function given by (2.9) with respect to $\hat{n}'$ which is the normal vector to the surface at the source point ρ', [38].

Assuming that the incident field is finite, the surface and the integration in (2.27) can be confined to a finite region, though the profile *C* is arbitrarily extended to infinity. Therefore, applying the same Method of

Moments (MoM) discretization process illustrated in Figure 2.2, the equivalent current density can be approximated, [2].

The Method of Moments Solution

The last integral equation (2.27) can be used to find the unknown induced current $J_t(\rho')$ based on the incident magnetic field $-H_y^{inc}(\rho)$. The solution may be reached numerically by reducing (2.27) to a series of linear algebraic equations that may be solved by customary matrix equations techniques. To facilitate this, the unknown current density $J_t(\rho')$ is approximated by an expansion of *N* known functions with constant, but unknown coefficients:

$$J_t(\rho') \cong \sum_{m=1}^{N} I_m p_m(\rho') \tag{2.28}$$

The $p_m(\rho')$ functions in the expansion (2.28) are chosen for their ability to accurately model the unknown quantity, while minimizing computation. They are often referred to as *basis* or expansion functions. To avoid the computational cost, subdomain piecewise constant or *pulse* functions will be used. These functions are defined to be of a constant value over one segment and zero elsewhere, such that

$$p_m(\rho') = \begin{cases} 1, & \text{if} \quad \rho' \in \text{segment } m \\ 0, & otherwise \end{cases} \tag{2.29}$$

The surface is now divided into *N* segments as illustrated in Figure 2.2. Note that, as $N \to \infty$, the approximated expression for the unknown current density approaches to the exact solution, [27,38].

Substituting (2.28) into (2.27) and evaluating (2.27) at a fixed observation point on the surface such as p_n, produces an integrand

that is solely a function of ρ'. Obviously this leads to one equation with N unknowns I_m. To obtain a solution for these N amplitude constants, N linearly independent equations are necessary. These equations may be produced by choosing an observation point p_n on the surface at the center of each segment as shown in Figure 2.2 (n =1, 2, …, N). This will result in one equation corresponding to each observation point. Thus,

$$-H_y^{inc}(\rho_n) \cong I_n + j\omega \in \sum_{m=1}^{N} I_m \int_{\Delta x_m} \eta_s(\rho_m) G(\rho_n, \rho_m) d\rho_m - \sum_{m=1}^{N} I_m \int_{\Delta x_m} \frac{\partial}{\partial n_m} G(\rho_n, \rho_m) d\rho_m \tag{2.30}$$

is valid for N such points of observation. The $N \times N$ system produced by (2.30) can be written more concisely using matrix notation as

$$-\begin{bmatrix} H_y^{inc}(\rho_1) \\ H_y^{inc}(\rho_2) \\ \vdots \\ H_y^{inc}(\rho_N) \end{bmatrix} = \begin{bmatrix} Z_{11} & Z_{12} & \cdots & Z_{1N} \\ Z_{21} & Z_{22} & \cdots & Z_{2N} \\ \vdots & \vdots & \ddots & \vdots \\ Z_{N1} & Z_{N2} & \cdots & Z_{NN} \end{bmatrix} \begin{bmatrix} I_1 \\ I_2 \\ \vdots \\ I_N \end{bmatrix} \tag{2.31}$$

or

$$[V_n] = [Z_{nm}] \cdot [I_m] \tag{2.32}$$

Consequently, the solution of (2.27) for the current distribution on a rough surface has been accomplished by approximating the unknown with pulse basis functions, dividing the surface into segments, and then sequentially enforcing (2.27) at the center of each segment (point matching) to form a set of linear equations, [2,27]. The entries of the MoM impedance matrix in (2.31) are given by

$$Z_{nm} = \int_{\Delta x_m} \left[j\omega \in \eta_m \, G(\rho_n, \rho_m) - \frac{\partial}{\partial n_m} G(\rho_n, \rho_m) \right] d\rho_m \tag{2.33}$$

where ρ_n denotes the observation point which is considered to be located on the center of the n^{th} segment, while ρ_m represents the source point on the center of the m^{th}. If the segments are small compared to the wavelength, typically $\lambda/10$, the elements of the impedance matrix may be approximated as,

$$Z_{nm} \cong \frac{\omega \in \eta_m}{4} \Delta x_m H_0^{(2)}\left(k\left|\rho_n - \rho_m\right|\right) + j\frac{k}{4}\Delta x_m H_1^{(2)}\left(k\left|\rho_n - \rho_m\right|\right)\hat{n}_m \cdot \hat{\rho}_{nm} \tag{2.34}$$

where $H_1^{(2)}$ is the Hankel function of the second-kind with order one, arising from the partial derivative of the Green's function and Δx_m is the length of the m^{th} segment. Also, $\hat{\rho}_{nm}$ denotes a unit vector in the direction from source ρ_m to the receiving element ρ_n, and $\hat{n}_m$ represents the unit normal vector of the surface at ρ_m.

Since the Hankel function is singular for $\rho_n = \rho_m$, the diagonal elements of the impedance matrix cannot be evaluated using (2.34). Moreover, the impedance matrix is diagonally dominant, and therefore using the small argument series expansion of the Hankel functions, diagonal entries of the impedance matrix can be obtained as, [27,39],

$$Z_{mm} \cong \frac{1}{2} + \frac{\omega \in \eta_m}{4}\Delta x_m \left[1 - j\frac{2}{\pi} ln\left(\frac{\gamma k \Delta x_m}{4e}\right)\right] \tag{2.35}$$

where γ is the Euler constant 1.781072418 and e = 2.718281828.

The expressions for the PEC case can be obtained simply by replacing η_m by 0. For the sake of completeness, the expressions for the PEC case are rewritten below:

$$Z_{nm} \cong j\frac{k}{4}\Delta x_m H_1^{(2)}\left(k\left|\rho_n - \rho_m\right|\right)\hat{n}_m \cdot \hat{\rho}_{nm} \tag{2.36}$$

$$Z_{mm} \cong \frac{1}{2} \tag{2.37}$$

The MoM procedure generates an impedance matrix that has N^2 entries for N surface unknowns. Each element of the matrix is calculated separately. For this reason, the processing time and memory requirement appears to be $O(N^2)$ to form the impedance matrix. Once the impedance matrix $\overline{\mathbf{Z}}$ is formed, the system $\mathbf{V} = \overline{\mathbf{Z}} \cdot \mathbf{I}$ should be solved for unknown current coefficients, $\mathbf{I} = \{I_m\}$, [27]. The direct solution method such as Gaussian elimination or LU decomposition requires an $O(N^3)$ floating point operations. Therefore, processing time for the solution becomes $O(N^3)$ for direct solution methods. As the problem size becomes electrically larger, computational requirements of the MoM increases very rapidly. The computational requirement for the problem under focus in this study is very high, and direct solution thechnique is prohibitively time-consuming due to dense impedance matrices. Therefore, instead of direct matrix inversion, gradient type iterative techniques such as CG (conjugate gradient) methods, whose formulation is given in Chapter 3, can be used to reduce the operation count to $O(N^2)$.

CHAPTER 3

A GRADIENT TYPE ITERATIVE SOLVER: CONJUGATE GRADIENT METHOD

3.1 Introduction

As mentioned in the previous chapter, the primary factor limiting the use of MoM in the calculation of electromagnetic scattering from rough surfaces is that a linear system of equations must be solved to obtain currents induced on the scatterer. Direct solution methods such as LU decomposition require $O(N^3)$ operations, where N is the number of unknowns in the discretized representation of the surface current. Electrically larger scattering surfaces (for very large N) increase the computational cost of the method and make it intractable especially at high frequencies.

The computational cost is reduced to $O(N^2)$ operations per iteration by using iterative techniques. The basic idea in iterative processes is to reach the exact solution by updating estimates at each iteration. Two different approaches can be applied as iterative schemes to solve the system of equations formed by MoM. These are, namely, stationary and non-stationary iterative techniques. In each of these methods, different update schemes are used for the estimates to find the exact solution, [27].

A method is called stationary if the rule to determine the estimates at each iteration does not change from iteration to iteration (i.e. the iteration matrix is stable during the process). In stationary iterative techniques, the surface current is approximated by physical optics approximation applied to the incident field, [40]. The current is then updated by applying surface boundary condition. Kapp and Brown, [41], and Holliday *et al.*, [15], choose the ordering of the updates to follow multiple scattering paths on the surface. This led Kapp and Brown and Holliday *et al.* to name their approaches as method of ordered multiple interactions (MOMI) and forward backward method (FBM), [38], respectively. These two techniques have shown a very effective and rapid convergence to solve linear systems of equations constructed by MFIE in vertical polarization case and EFIE in horizontal polarization case for the PEC and non-PEC surfaces, which are single valued and rough in one dimension. But when the ordering of the scatterer is multi-valued (re-entrant surfaces), divergence problem occurs, [37].

Non-stationary techniques are the second kind of iterative methods used to solve systems formed by MoM solution. These methods are extensions of standard conjugate gradient (CG) method, [16], which converge to the exact solution assuming infinite precision by constructing orthogonal vector sequences. The bi-conjugate gradient (BiCG) method used in [17], the generalized conjugate gradient (GCG) method utilized in [18] and the quasi-minimum residual (QMR) method employed in [20] are some typical examples. These methods are developed to solve asymmetric/non-Hermitian complex linear systems of equations and hence, their algorithms are different than those of stationary methods. In these kinds of methods, the rule to determine the estimates changes from iteration to iteration. The rule is based on

orthogonality conditions in the space defining the linear system of equations. Consequently, a new iteration matrix is generated at every iteration step to update the estimates, [37].

This chapter is devoted to the discussion of conjugate gradient method. And the evaluation of induced currents on some terrain surfaces. Next chapter is devoted to the acceleration of the algorithm by performing the matrix-vector multiplications faster. The properties of conjugate gradient methods are presented and numerical results for CG method are given in the following sections.

3.2 Conjugate Gradient (CG) Method

The conjugate gradient method, which is the oldest and best, known nonstationary technique, is an effective method for symmetric positive definite systems. This method is developed to solve a linear system of equations given by $\overline{\mathbf{A}}\,\mathbf{x} = \mathbf{b}$, where $\overline{\mathbf{A}}$ is an *N*x*N* interaction matrix, **b** is an excitation vector for the system and **x** is the unknown vector to be solved. The process, which stimulates the method is the generation of vector sequences of iterates (i.e., consecutive approximations to the solution), creating residuals that correspond to the iterates, and search directions that are used to update the iterates and residuals. Although the length of these sequences can become large, only a small number of vectors are needed to be kept in memory. In order to calculate update scalars that are defined to assure that the sequences fulfill certain orthogonality conditions, there are two inner products to be used at each iteration of the method. These conditions guarantee on a symmetric positive definite linear system that the distance to the true solution is minimized according to some standards, [27].

Peterson, Ray and Mittra give very detailed information for the method in their book chapters, [27,42]. It is necessary to define an inner product, and they employ the conventional Euclidean scalar product

$$\langle \mathrm{x}, \mathrm{y} \rangle = \mathrm{x}^{\dagger} \mathrm{y} \tag{3.1}$$

and its associated norm

$$\| \mathrm{x} \| = \sqrt{\langle \mathrm{x}, \mathrm{x} \rangle} \tag{3.2}$$

where the dagger "†" denotes the transpose-conjugate of a matrix.

All iterative algorithms for solving $\overline{\mathbf{A}}\,\mathbf{x} = \mathbf{b}$ seek an estimate of the solution in the form

$$\mathbf{x}_n = \mathbf{x}_{n-1} + \alpha_n \mathbf{p}_n \tag{3.3}$$

where $\mathbf{x}_{n-1}$ is a previous estimate of the solution, $\mathbf{p}_n$ is a "direction" vector ($\mathbf{p}_n$ determines the direction in the N-dimensional space in which the algorithm moves to correct the estimate of $\mathbf{x}$), and α_n is a scalar coefficient that determines how far the algorithm moves in the $\mathbf{p}_n$ direction. Altough all iterative methods are similar in that they follow the form of (3.3), they differ in the procedure by which they generate α_n and $\mathbf{p}_n$. Nondivergence can be guaranteed by selecting α_n in order to minimize an error functional. The CG algorithm to be presented is based on the error functional

$$E_n(\mathbf{x}_n) = \| \mathbf{A}\mathbf{x}_n - \mathbf{b} \|^2 \tag{3.4}$$

Note that other functionals have been used and give rise to related members of the family of CG algoritms, [42].

The coefficient α_n from (3.3) that minimizes the functional is given by

$$\alpha_n = \frac{-\langle \mathbf{A}\mathbf{p}_n, \mathbf{r}_{n-1} \rangle}{\| \mathbf{A}\mathbf{p}_n \|^2} \tag{3.5}$$

where for convenience the residual vector is

$$\mathbf{r}_n = \mathbf{A}\mathbf{x}_n - \mathbf{b} \tag{3.6}$$

This process has the geometric interpretation of minimizing E_n along the line in N-dimensional space defined by $\mathbf{p}_n$, [27].

It is resonable to expect that an improved algorithm would seek the minimum of E_n in a plane spanned by two direction vectors. For example, consider a solution estimate of the form

$$\mathbf{x}_n = \mathbf{x}_{n-1} + \alpha_n (\mathbf{p}_n + \beta_n \mathbf{q}_n) \tag{3.7}$$

where the direction vectors $\mathbf{p}_n$ and $\mathbf{q}_n$ span a plane in N-dimensional space and the scalar coefficients α_n and β_n are to be obtained to simultaneously minimize the error functional E_n. Carrying out the simultaneous minimization, α_n is given by (3.5) with $\mathbf{p}_n$ replaced by $\mathbf{p}_n+\beta_n\mathbf{q}_n$ and β_n is given by

$$\beta_n = \frac{\langle \mathbf{A}\mathbf{q}_n, \mathbf{r}_{n-1} \rangle \|\mathbf{A}\mathbf{p}_n\|^2 - \langle \mathbf{A}\mathbf{p}_n, \mathbf{r}_{n-1} \rangle \langle \mathbf{A}\mathbf{q}_n, \mathbf{A}\mathbf{p}_n \rangle}{\langle \mathbf{A}\mathbf{p}_n, \mathbf{r}_{n-1} \rangle \|\mathbf{A}\mathbf{q}_n\|^2 - \langle \mathbf{A}\mathbf{q}_n, \mathbf{r}_{n-1} \rangle \langle \mathbf{A}\mathbf{p}_n, \mathbf{A}\mathbf{q}_n \rangle} \tag{3.8}$$

Suppose that $\mathbf{p}_n$ and $\mathbf{q}_n$ are arbitrary direction vectors but that $\mathbf{q}_n$ has been previously used in the iterative procedure, so that

$$\mathbf{x}_{n-1} = \mathbf{x}_{n-2} + \alpha_{n-1} \mathbf{q}_n \tag{3.9}$$

where α_{n-1} was previously found to minimize the error functional along the line defined by $\mathbf{q}_n$, that is,

$$\alpha_{n-1} = \frac{-\langle \mathbf{A}\mathbf{q}_n, \mathbf{r}_{n-2} \rangle}{\|\mathbf{A}\mathbf{q}_n\|^2} \tag{3.10}$$

It immediately follows that

$$\langle \mathbf{A}\mathbf{q}_n, \mathbf{r}_{n-1} \rangle = \langle \mathbf{A}\mathbf{q}_n, \mathbf{r}_{n-2} + \alpha_{n-1}\mathbf{A}\mathbf{q}_n \rangle = 0 \tag{3.11}$$

$$\beta_n = \frac{-\langle \mathbf{A}\mathbf{q}_n, \mathbf{A}\mathbf{p}_n \rangle}{\|\mathbf{A}\mathbf{q}_n\|^2} \tag{3.12}$$

and

$$\langle \mathbf{A}(\mathbf{p}_n + \beta_n \mathbf{q}_n), \mathbf{A}\mathbf{q}_n \rangle = 0 \tag{3.13}$$

Therefore, if the solution is already optimized along the $\mathbf{q}_n$ direction, the best solution in the plane spanned by $\mathbf{p}_n$ and $\mathbf{q}_n$ is obtained in a direction orthogonal to $\mathbf{q}_n$ in the sense of (3.13), [42].

This analysis shows that the process of selecting direction vectors and coefficients to minimize the error functional E_n is optimized when vectors satisfying the orthogonality condition

$$\left\langle \mathbf{A}\,\mathbf{p}_i\,, \mathbf{A}\mathbf{p}_j \right\rangle = 0 \qquad i \neq j \tag{3.14}$$

are used. If an arbitrary set of direction vectors is employed, the process of minimizing E_n will adjust their coefficients in order to generate a sequence satisfying this generalized orthogonality. Furthermore, if direction vectors satisfying (3.14) are used, there is no advantage in simultaneously minimizing the error functional along more than one direction. Vectors satisfying (3.14) are said to be mutually conjugate with respect to the operator $\mathbf{A}^\dagger\mathbf{A}$, where $\mathbf{A}^\dagger$ is the adjoint with respect to the inner product, that is,

$$\left\langle \mathbf{A}^\dagger\mathbf{x}, \mathbf{y} \right\rangle = \left\langle \mathbf{x}, \mathbf{A}\mathbf{y} \right\rangle \tag{3.15}$$

In accordance with the definition for the inner product above, the matrix $\mathbf{A}^\dagger$ is the transpose conjugate of $\mathbf{A}$, [27]. It is shown in [27] that a set of direction vectors satisfying the orthogonality condition of (3.14) is available. Since $\mathbf{A}$ is nonsingular, these vectors are linearly independent and span the N-dimensional space. The solution can be expressed in the form

$$\mathbf{x} = \mathbf{x}_0 + \alpha_1\mathbf{p}_1 + \alpha_2\mathbf{p}_2 + \cdots + \alpha_N\mathbf{p}_N \tag{3.16}$$

where, the arbitrary vector $\mathbf{x}_0$ can be thought of as an initial estimate, or "guess", for the solution $\mathbf{x}$. Because of the orthogonality stated in (3.14), each coefficient can be found independently according to

$$\alpha_n = \frac{-\left\langle \mathbf{A}\mathbf{p}_n, \mathbf{r}_0 \right\rangle}{\left\| \mathbf{A}\mathbf{p}_n \right\|^2} \tag{3.17}$$

where $\mathbf{r}_0 = \mathbf{A}\mathbf{x}_0 - \mathbf{b}$.

From the above relationships, it is apparent that

$$\mathbf{r}_n = \mathbf{r}_0 + \alpha_1\mathbf{A}\mathbf{p}_1 + \alpha_2\mathbf{A}\mathbf{p}_2 + \cdots + \alpha_N\mathbf{A}\mathbf{p}_N \tag{3.18}$$

and recursive relations are given as

$$\mathbf{r}_n = \mathbf{r}_{n-1} + \alpha_n \mathbf{A}\mathbf{p}_n \tag{3.19}$$

$$\mathbf{x}_n = \mathbf{x}_{n-1} + \alpha_n \mathbf{p}_n \tag{3.20}$$

and

$$\left\| \mathbf{r}_n \right\|^2 = \left\| \mathbf{r}_{n-1} \right\|^2 - \left| \alpha_n \right|^2 \left\| \mathbf{A}\mathbf{p}_n \right\|^2 \tag{3.21}$$

From (3.14), (3.17) and (3.18) it can be deduce that, [27]

$$\left\langle \mathbf{A}\mathbf{p}_m, \mathbf{r}_n \right\rangle = \begin{cases} \left\langle \mathbf{A}\mathbf{p}_m, \mathbf{r}_0 \right\rangle & n \le m \\ 0 & n \ge m \end{cases} \tag{3.22}$$

It follows that equations in (3.5) and in (3.17) are equivalent, indicating that the error minimization process and the orthogonal expansion procedure yield the same results.

The process of expanding a solution in terms of mutually conjugate direction vectors is known as the *conjugate direction method*, after Hestenes and Stiefel, [27, 43]. Peterson et al. state that the conjugate direction method does not specify the means for generating mutual conjugate sequence, [27]. The CG method is a conjugate direction method that includes a recursive procedure, for generating the $\mathbf{p}$ vectors. The CG algorithm begins with the choice

$$\mathbf{p}_1 = -\mathbf{A}^\dagger \mathbf{r}_0 \tag{3.23}$$

which is proportional to the gradient of the functional E_n at $\mathbf{x} = \mathbf{x}_0$. Subsequent functions are found from

$$\mathbf{p}_{n+1} = -\mathbf{A}^\dagger \mathbf{r}_n + \beta_n \mathbf{p}_n \tag{3.24}$$

where the scalar coefficient β_n is chosen to ensure

$$\left\langle \mathbf{A}^{\dagger}\mathbf{A}\mathbf{p}_n, \mathbf{p}_{n+1} \right\rangle = 0 \tag{3.25}$$

Peterson et al demonstrate that enforcing (3.25) is sufficient to ensure that the **p** vectors form a mutually conjugate set satisfying (3.14) [27]. To illustrate, they first present several relationships involving the vectors generated within the CG algorithm.

From (3.24),

$$\left\langle \mathbf{A}^{\dagger}\mathbf{r}_m, \mathbf{p}_{n+1} \right\rangle = -\left\langle \mathbf{A}^{\dagger}\mathbf{r}_m, \mathbf{A}^{\dagger}\mathbf{r}_n \right\rangle + \beta_n \left\langle \mathbf{A}^{\dagger}\mathbf{r}_m, \mathbf{p}_n \right\rangle \tag{3.26}$$

According to (3.22), the first and last inner product in (3.26) vanish for $m > n$, leaving

$$\left\langle \mathbf{A}^{\dagger}\mathbf{r}_n, \mathbf{A}^{\dagger}\mathbf{r}_m \right\rangle = 0 \qquad m \neq n \tag{3.27}$$

which is the orthogonality associated with the residual vectors. (3.22) and (3.24) can be combined to produce

$$\left\langle \mathbf{p}_{n+1}, \mathbf{A}^{\dagger}\mathbf{r}_n \right\rangle = -\left\langle \mathbf{A}^{\dagger}\mathbf{r}_n, \mathbf{A}^{\dagger}\mathbf{r}_n \right\rangle = -\left\| \mathbf{A}^{\dagger}\mathbf{r}_n \right\|^2 \tag{3.28}$$

Therefore, α_n can be expressed in the alternate form

$$\alpha_n = \frac{\left\| \mathbf{A}^{\dagger}\mathbf{r}_{n-1} \right\|^2}{\left\| \mathbf{A}\mathbf{p}_n \right\|^2} \tag{3.29}$$

From (3.19),

$$\mathbf{A}^{\dagger}\mathbf{r}_n = \mathbf{A}^{\dagger}\mathbf{r}_{n-1} + \alpha_n \mathbf{A}^{\dagger}\mathbf{A}\mathbf{p}_n \tag{3.30}$$

Because of the orthogonality expressed in (3.27), an inner product between $\mathbf{A}^{\dagger}\mathbf{r}_m$ and (3.30) leads to the result

$$\left\langle \mathbf{A}^{\dagger}\mathbf{r}_m, \mathbf{A}^{\dagger}\mathbf{A}\mathbf{p}_n \right\rangle = \begin{cases} \dfrac{\left\| \mathbf{A}^{\dagger}\mathbf{r}_m \right\|^2}{\alpha_n} & m = n \\ -\dfrac{\left\| \mathbf{A}^{\dagger}\mathbf{r}_m \right\|^2}{\alpha_n} & m = n - 1 \\ 0 & \text{otherwise} \end{cases} \tag{3.31}$$

Using (3.31) with $m = n$, the value of β_n can be found from (3.24) and (3.25) as

$$\beta_n = \frac{\left\| \mathbf{A}^\dagger \mathbf{r}_n \right\|^2}{\left\| \mathbf{A}^\dagger \mathbf{r}_{n-1} \right\|^2} \quad . \tag{3.32}$$

In an inductive fashion one can see that the direction vectors generated by the procedure satisfy the assumed orthogonality properties of the conjugate direction method.

In the computer science literature, this particular form of the CG algorithm is referred to as the "conjugate gradient method applied to the normal equations". The conventional CG algorithm discussed in many texts is restricted to the special case of a Hermitian positive-definite matrix **A**. The authors of [27] say that to extend algorithm to arbitrary linear systems, the matrix equation is premultiplied by $\mathbf{A}^\dagger$ to produce the normal equations $\mathbf{A}^\dagger\mathbf{A}\mathbf{x} = \mathbf{A}^\dagger\mathbf{b}$. Note that it is not necessary to compute the product explicitly, and a variety of related CG algorithms can be constructed based on this equation, [44].

For an arbitrary nonsingular matrix **A**, the CG algorithm outlined above produces a solution in at most N iteration steps (assuming infinite-precision arithmetic). This is a direct consequence of the fact that N **p**-vectors span the solution space. Finite-step termination is a significant advantage of the CG method over other iterative algorithms. In addition, the CG algorithm produces solution estimates that satisfy

$$\left\| \mathbf{x} - \mathbf{x}_n \right\| \leq \left\| \mathbf{x} - \mathbf{x}_m \right\| \qquad n > m \tag{3.33}$$

In words, the error in $\mathbf{x}_n$ decreases monotonically as the algorithm progress. Consequently, it will usually be possible to terminate the algorithm prior to the n^{th} iteration step, [27]. For the purpose of

terminating the CG algorithm, it is necessary to estimate the accuracy of $\mathbf{x}_n$ at each step. Since the solution $\mathbf{x}$ is not known, the error vector

$$\mathbf{e}_n = \mathbf{x} - \mathbf{x}_n \tag{3.34}$$

is not directly computable. Instead, it is convenient to compute the residual norm

$$N_n = \frac{\|\mathbf{r}_n\|}{\|\mathbf{b}\|} = \frac{\|\mathbf{A}\mathbf{x}_n - \mathbf{b}\|}{\|\mathbf{b}\|} \tag{3.35}$$

As illustrated by (3.21), the residual norm decreases monotonically (a direct consequence of minimizing E_n at each iteration step). The CG algorithm can be terminated when the residual norm decreases to some predetermined value. As long as $\mathbf{A}$ is fairly well conditioned, $N_n<10^{-4}$ suggests that several decimal places of accuracy are obtained in $\mathbf{x}_n$. However, note that the residual norm only provides an indirect bound on the error, [45]. Peterson et al. warn that if the matrix $\mathbf{A}$ becomes ill conditioned, the residual norm, N_n, may be a poor indication of the accuracy of $\mathbf{x}_n$. If the matrix is poorly conditioned, the convergence may be slow, [27].

In infinite-precision arithmetic, the CG algorithm produces a solution in at most N iteration steps. Unfortunately, for a general linear system, CG requires approximately six times the number of operations as LU factorization to attain N complete steps. Thus, to be competitive with direct methods, the CG algorithm would have to converge to necessary accuracy in fewer than N/6 iteration steps. Consequently, the CG algorithm is usually reserved for treating matrix equations having sparsity or special structure that cannot easily be exploited using direct methods of solution. Because the integral equations of electromagnetics involve convolutional kernels, the matrix equations of interest often possess discrete-convolutional symmetries, [27]. An

implementation of the CG method for treating these systems is discussed in next chapter.

3.3 Numerical Results For Conjugate Gradient (CG) Method

In this section, some numerical results are presented to validate the convergence and accuracy of the Conjugate Gradient Method over one-dimensional rough terrain profiles. Applying method of moments, a matrix equation is formed to obtain the unknown current coefficients

$$\overline{\mathbf{Z}} \cdot \mathbf{I} = \mathbf{V} \tag{3.36}$$

where the elements of the impedance matrices are given by (2.20) and (2.21) for TM polarization and by (2.35) and (2.37) for TE polarization, respectively. Results are obtained both for perfect and imperfect conductor surfaces. In order to check the accuracy of the method, results are compared with the direct solution of the method of moment's matrix equation. The pulse width in point matching technique is taken as x = λ / 10. Residual error is employed as a stopping criterion of the iterative method. The residual error vector at the i^{th} iteration step is defined as

$$\mathbf{r}^i = \mathbf{V} - \overline{\mathbf{Z}} \cdot \mathbf{I}^i \tag{3.37.a}$$

and the corresponding residual error is given as,

$$residual\ error = \frac{\left\| \mathbf{r}^i \right\|}{\left\| \mathbf{V} \right\|} \tag{3.37.b}$$

where || **.** || denotes the vector norm. The stopping criterion of the CG method is limited by the residual error of 10^{-4} in this thesis. It has been seen that this error rate is sufficient to obtain accurate results.

3.3.1 Source Incidence on the Terrain Profile

Three kinds of sources are considered in the thesis. The first one is finite plane wave excitation as shown in Figure 3.1(a). The elements of the excitation vector for the TM polarization will be

$$v_n = E^i(\rho_n) = \begin{cases} -e^{-jk(x_n\cos\theta - z_n\sin\theta)} & \text{,on the surface} \\ 0 & \text{,elsewhere} \end{cases} \tag{3.38}$$

where the subscript *n* denotes the location of observation points on the terrain. For the TE polarization, it can be expressed as

$$v_n = -H^i(\rho_n) = \frac{1}{\eta_0}\begin{cases} -e^{-jk(x_n\cos\theta - z_n\sin\theta)} & \text{,on the surface} \\ 0 & \text{,elsewhere} \end{cases} \tag{3.39}$$

The second source is an isotropic radiator located above the surface as shown in Figure 3.1(b). The elements of the of the excitation vector for TM and TE cases are

$$v_n = -E^i(\rho_n) = -E_0\frac{e^{-jkd_n}}{d_n} \tag{3.40}$$

and

$$v_n = -H^i(\rho_n) = -\frac{E_0}{\eta_0}\frac{e^{-jkd_n}}{d_n} \tag{3.41}$$

respectively. The source distance d_n is

$$d_n = \sqrt{(x_n - x_s)^2 + (z_n - z_s)^2} \tag{3.42}$$

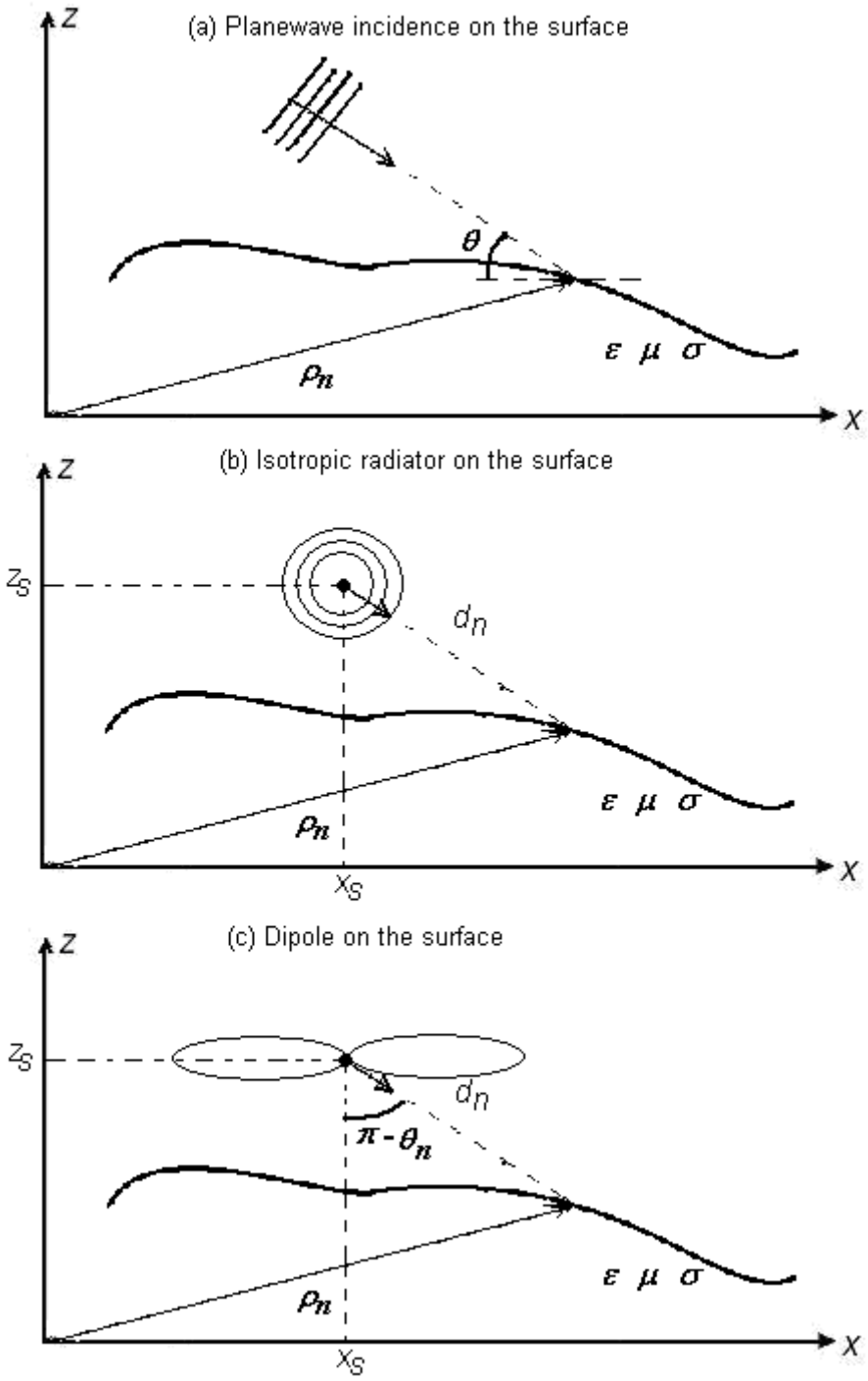

Figure 3.1: Source incidence on the terrain profile

The last source considered here is an infinitesimal dipole depicted in Figure 3.1(c). For this type of excitation, elements of the incident field vector for both vertical and horizontal polarizations are:

$$v_n = -E^i(\rho_n) = -E_0 \frac{e^{-jkd_n}}{d_n} \sin\theta_n \tag{3.43}$$

and

$$v_n = -H^i(\rho_n) = -\frac{E_0}{\eta_0} \frac{e^{-jkd_n}}{d_n} \sin\theta_n \tag{3.44}$$

where

$$\sin\theta_n = \frac{x_n - x_s}{d_n} \tag{3.45}$$

3.3.2 Applications of CG Method over Rough Surfaces

Operating frequency is chosen to be 10 GHz, which corresponds to 3 centimeters wavelength for all of the results, and the radiated power is chosen as 100 Watts. Figure 3.2 shows a strip surface of width 50λ.

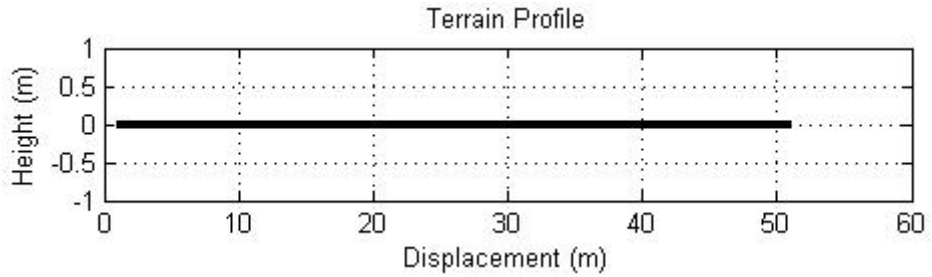

Figure 3.2: Strip surface of width 50λ

Plane wave incidence is considered for both TM and TE polarizations. Figure 3.3 shows results for oblique ($\theta = \pi/2$) incidence. To see the absorption effects of the terrain profile, both PEC ($\eta_s = 0$) and imperfect conducting case are considered. For the non-PEC case the

surface impedance is taken as $\eta_s = 15 + \mathrm{j}20$ as an example. The non-PEC case is considered just for the sake of completeness since the earth behaves like a PEC at x-band frequencies. As can be seen in Figure 3.3(c), the TE polarized plane wave, induced on the strip for the PEC case, results a stable current on the terrain profile. The interaction matrix is a diagonal matrix. Using (2.37) one can easily see that the self-terms are ½ and (since $\eta_m = 0$) and the mutual terms are 0 since the unit vector $\hat{n}_m$ is always perpendicular to the surface of the strip. This shows that the tangential current in the MFIE is:

$$J_t(\rho) = -2H^i(\rho) \tag{3.46}$$

This is a reasonable result considering that the surface profile is extended to infinity, thus the induced current on an infinite strip is the physical optics current $\mathbf{J}_s^{PO} = 2\hat{\mathrm{n}} \times \mathbf{H}^{inc}$. Hence, reaching accurate solution of the induced current over flat PEC strip profiles for vertical polarization is not numerically possible. However, when the strip is imperfectly conducting, the MFIE yields accurate results as shown in Figure 3.3(d). This is also true when we are dealing with undulating geometries that the dot product term in (3.36), to find mutual elements interaction, does not vanish.

Figure 3.4 illustrates the residual errors of Figure 3.3(a) and Figure 3.3(b). It can be clearly seen in Figure 3.4(a) and Figure 3.4(b) that non-PEC case reaches at the desired level of error in a faster way.

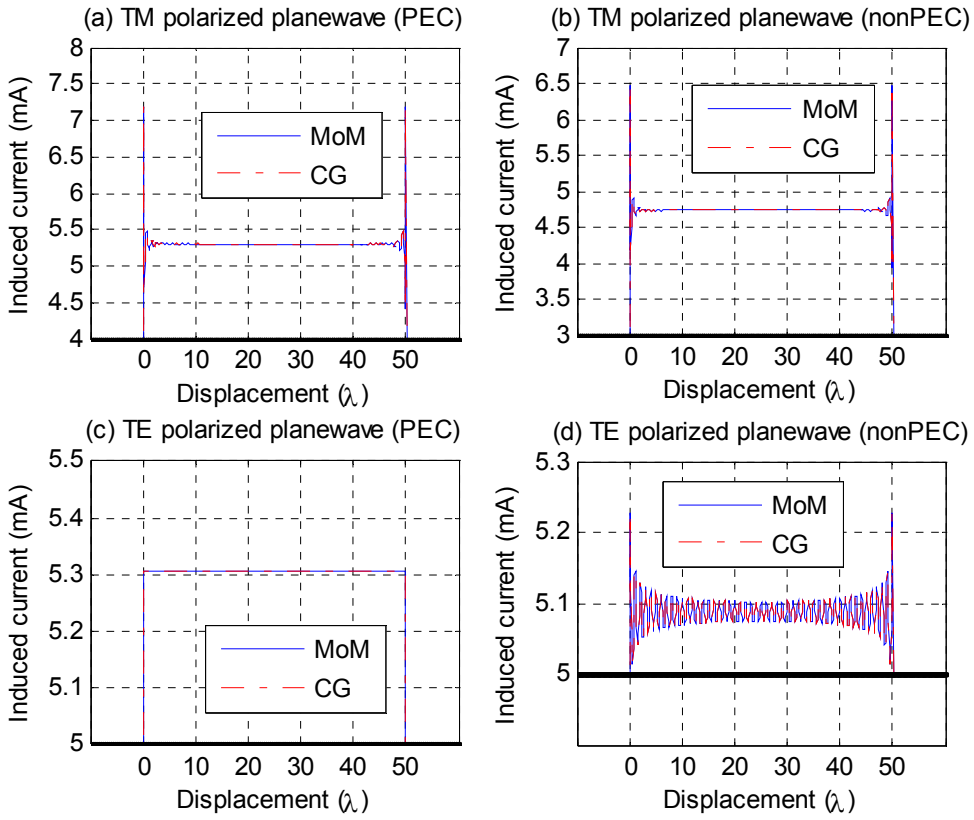

Figure 3.3: Distributed current on a strip, oblique plane wave incidence

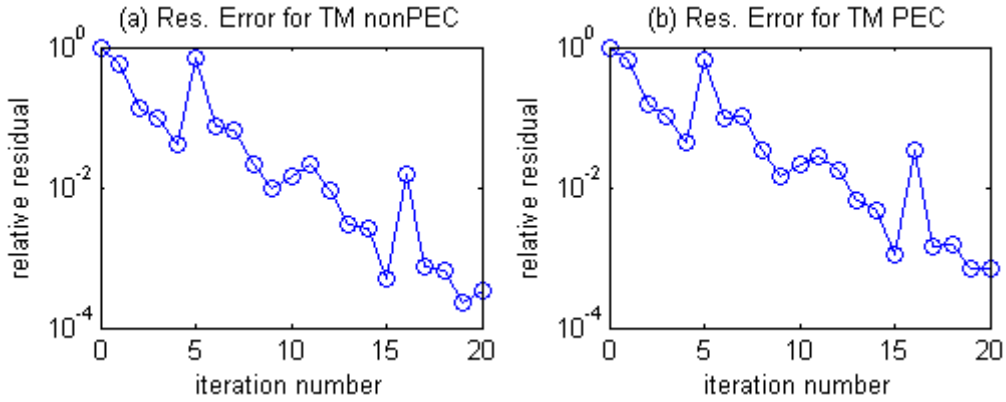

Figure 3.4: Residual errors for TM polarized case for PEC and Non-PEC

A rough surface profile of width 100λ illuminated by a plane wave is shown in Figure 3.5 for both polarization cases. Maximum height deviation is about 20λ. The incident angle is now $\theta = \pi/20$ (grazing incidence). Results show that the CG method solution converges more successfully than direct solution of MoM. Because of grazing angle condition, shadowing effects are seen after the hill of the terrain.

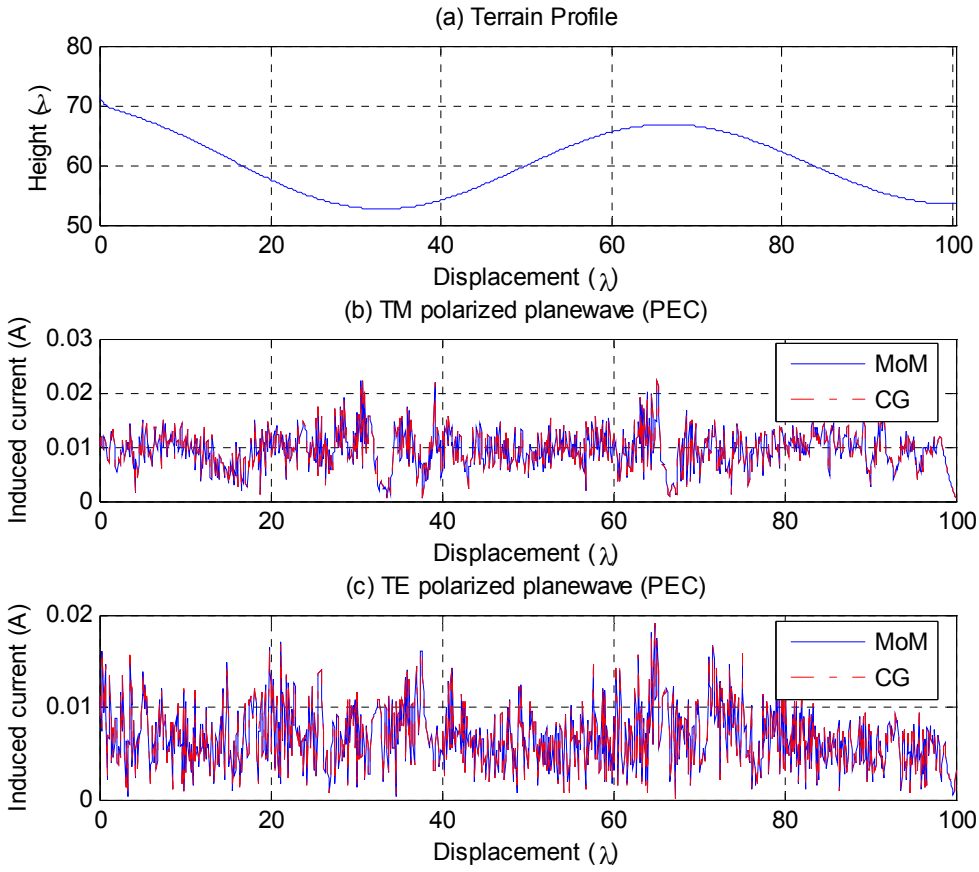

Figure 3.5: Distributed current on a 100λ rough surface, grazing plane wave

The residual errors with respect to the iteration number are given in Figure 3.6. The desired level of error is achieved in less iterations for

the TM PEC case. Figure 3.7 shows the third example in which the terrain is again a 100λ long rough surface illuminated by an isotropic radiator placed at 25λ above the left most point of the terrain. The radiated power is assumed to be 25 Watts. Both TM and TE polarization cases are plotted for perfect conducting surface in Figure 2.7.

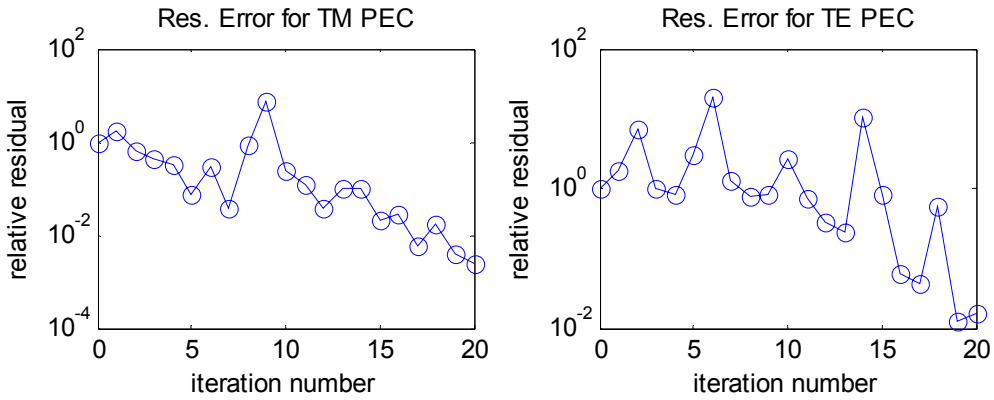

Figure 3.6: Residual errors of Figure 3.5

The residual errors with respect to the iteration number are given in Figure 3.8. Again, the desired level of error is achieved in less iterations for the TM PEC case in which occurs at the 9th iteration.

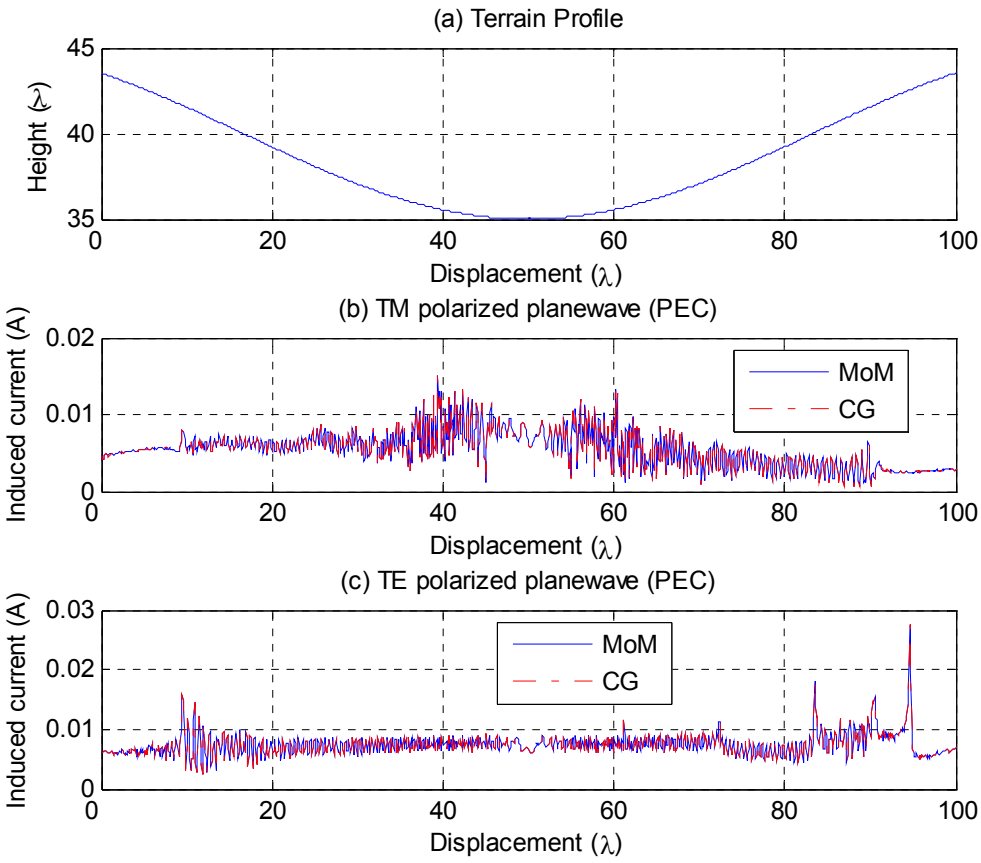

Figure 3.7: Isotropic radiator on the rough surface

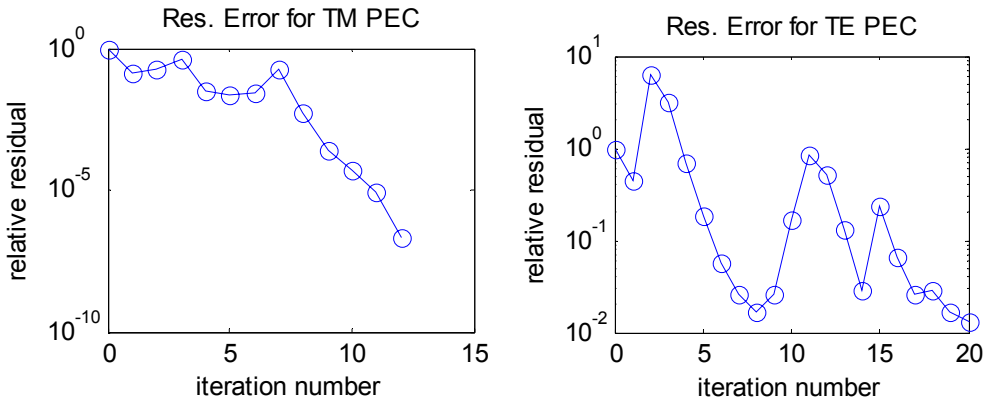

Figure 3.8: Residual errors of Figure 3.7

Figure 3.9 displays a rough surface of length 200λ. The results are again compared with direct MoM solution for validity. An infinitesimal dipole is placed above the surface at a height of 25λ at the center of the terrain. The surface impedance of non-PEC surface is taken as $\eta_s = 15 + j20$. The radiated power is chosen as 25 Watts. Because of the hill geometry, and the antenna position the current suddenly decreases between 90 centimeters and 1.8 meters and also between 3.6 meters and 3.9 meters. This is the shadowing effect of the peak of the terrain preceding the location of the dipole. The left lobe of the current is slightly higher than the right one due to θ_n deviation.

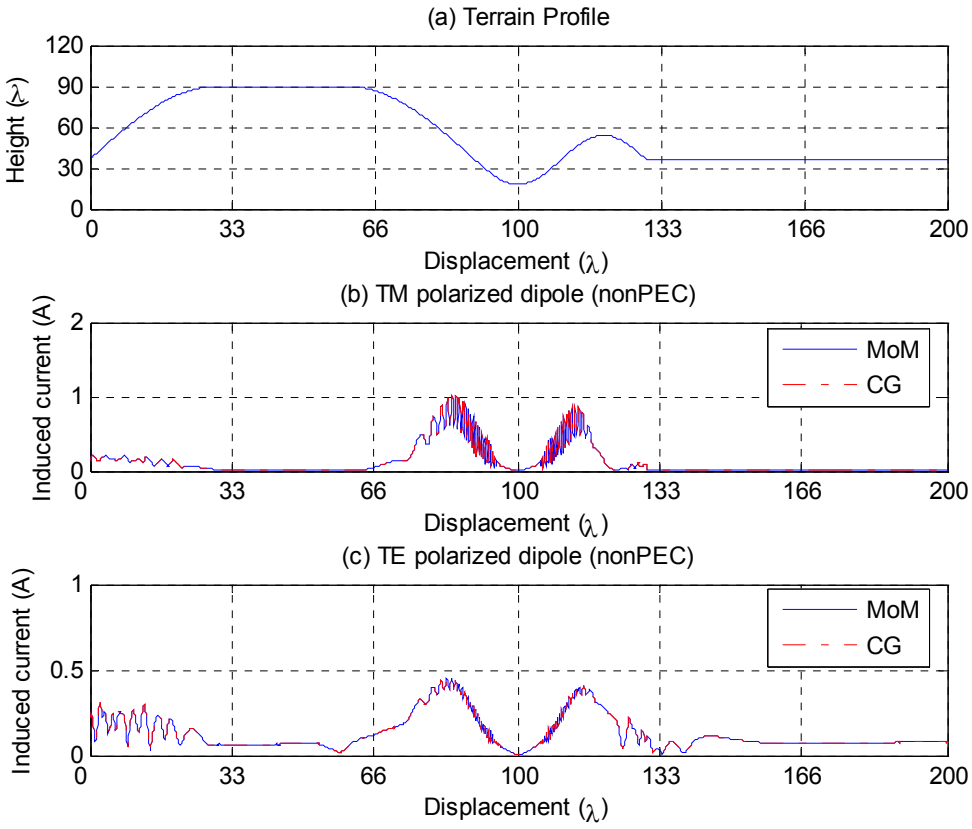

Figure 3.9: Dipole radiator on the rough surface located at the center of terrain profile

Figure 3.10 shows same surface profile of length 200λ, in which, imperfectly conducting surface case is considered with $\eta_s = 25 + j20$. Dipole antenna is located at 1 meters (~33 λ) on the displacement axis 10 λ above the surface.

Average radiated power is now 30 Watts. The shadowing effects are clearly seen on the surface. And the oscillations are also clearly seen in Figure 3.10 (b) and Figure 3.10 (c). It must be noted that the induced current is oscillating in the flat region at right side of the surface profile and its magnitude decreases as the distance to the antenna increases.

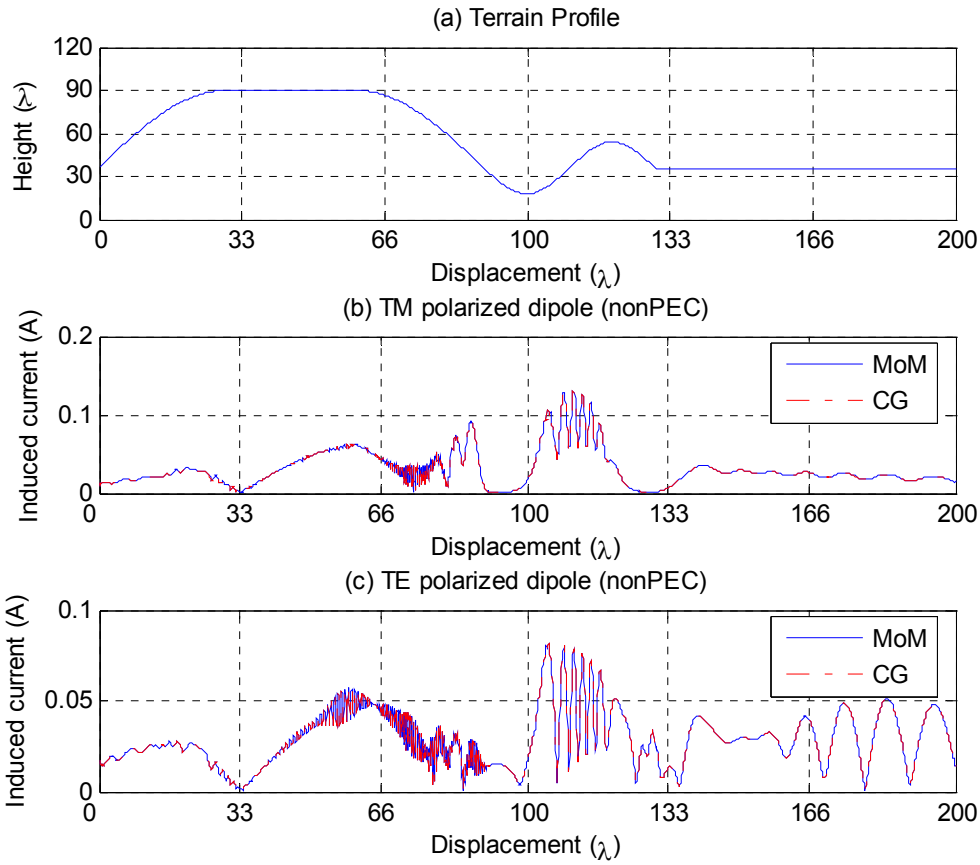

Figure 3.10: Dipole radiator on the rough surface located at the 33λ point on the terrain profile

Figure 3.11 illustrates a quasi-planar surface profile of length 200 λ. Surface impedance of imperfect conducting case is chosen to be $\eta_s = 25 + j20$. Dipole antenna is located at 4.5 meters (150 λ) on the displacement axis 10 λ above the surface. Average radiated power is 10 Watts for this case.

The shadowing effects are clearly seen on the surface. One can also see that the current magnitude is decreasing inversely by the distance to the source in the flat regions of the surface profile and shows similar behaviour of dipole on the rough surface in Figure 3.9.

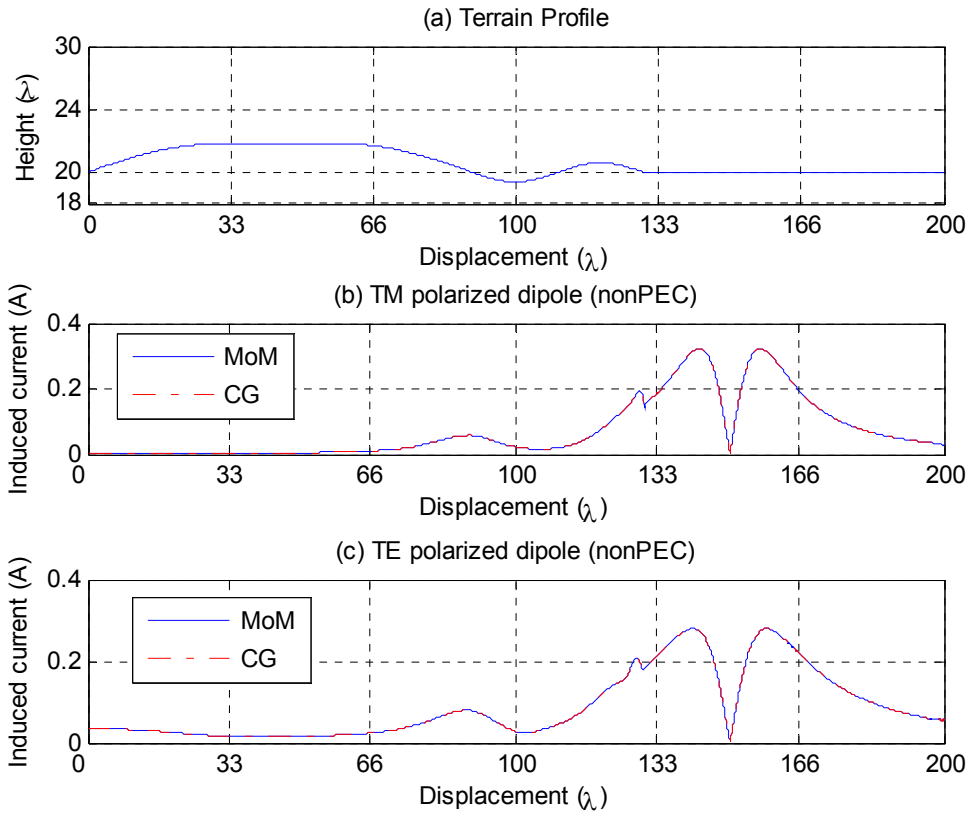

Figure 3.11: Dipole on a quasi-planar surface of width 200λ

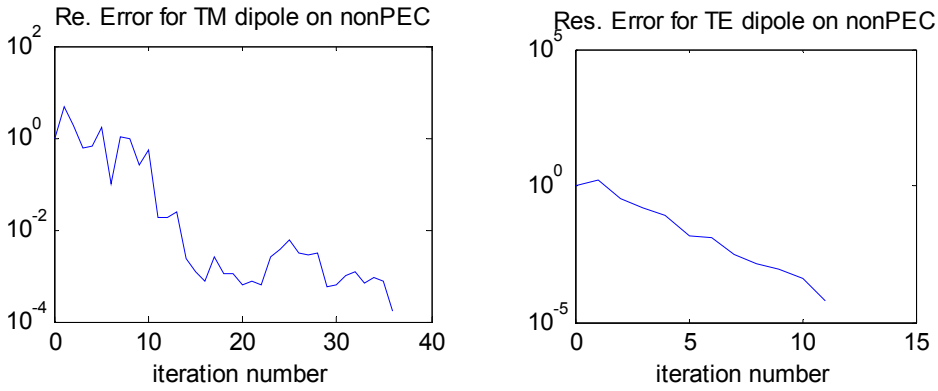

Figure 3.12: Residual errors of Figure 3.11

The residual errors with respect to the iteration number are given in Figure 3.12 for both TM case and TE case. The desired residual error constraint, which is 10^{-4}, is achieved in only 11 iterations for the TE non-PEC case. Another important thing is that the residual error decreases monotonically in each iteration step for TE case.

The last example is sea surface profile. Imperfect conducting case is considered in which the sea is assumed to have a surface impedance of $\eta_s = 76.4 - j65.1$ and relative permitivity of sea is chosen as 78. Plane wave incidence is considered with an incidence angle of $\theta = \pi/30$.

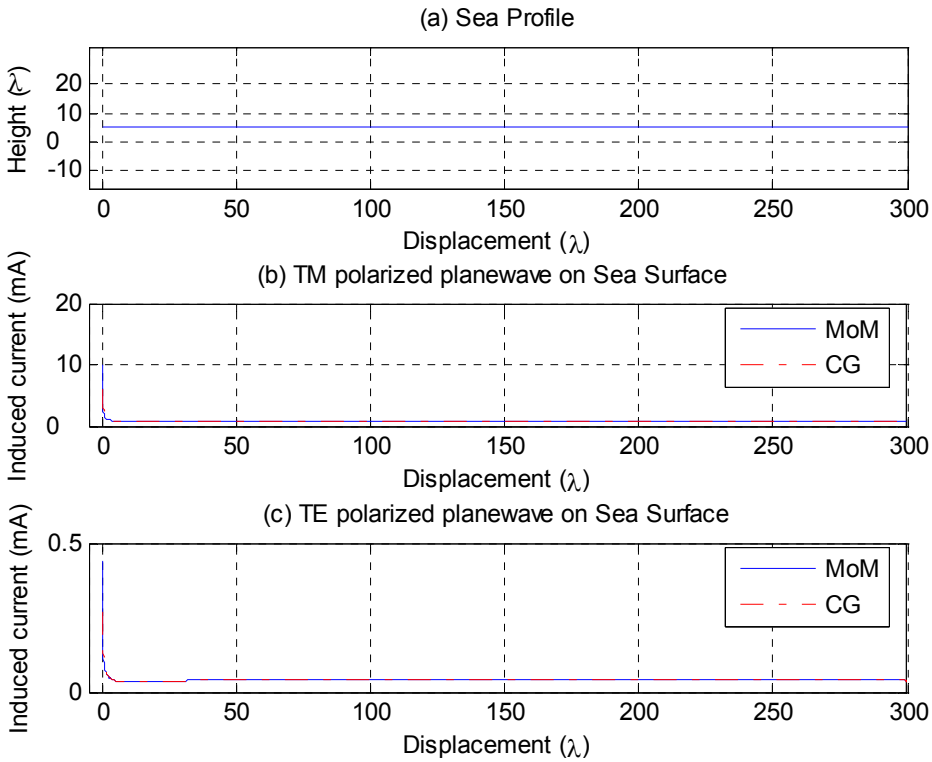

Figure 3.13: Distributed current on a 300λ rough surface, grazing plane wave

Current distributions on the surface of the sea due to 0 m/s wind speed are plotted in Figure 3.13. The frequency is 10 GHz with *N*=3000. The residual errors with respect to the iteration number are given in Figure 3.14 for both TM case and TE case. Again, the desired residual error is achived in less number of iterations for the TE non-PEC case. The desired level of error is reached at the 135th iteration step.

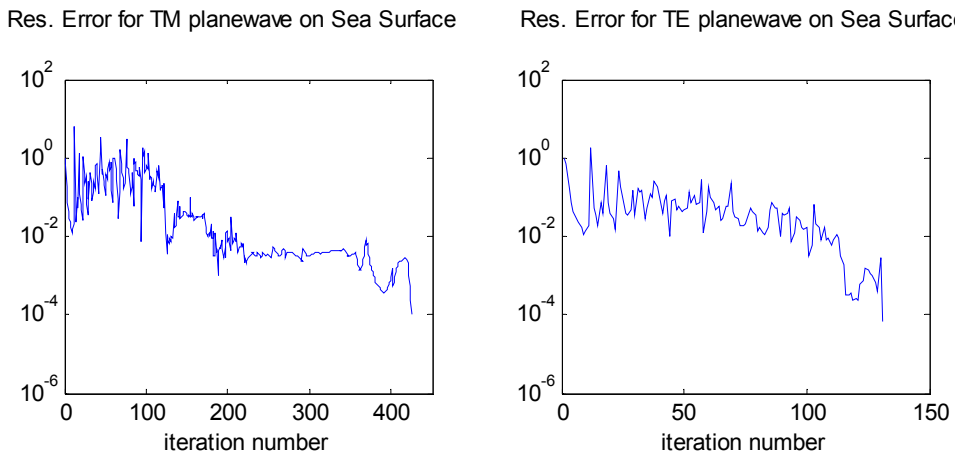

Figure 3.14: Residual errors of Figure 3.13

N = 3000 is the upper limit to use direct matrix inversion with MoM as a reference due to RAM requirement of the computer used. Also the operation count of $O(N^3)$ to employ LU decomposition to invert the MoM matrix makes the process really cumbersome after this number of unknowns. The numerical examples show that CG method is well suited for scattering problems. By applying this method, the operation count is reduced to $O(N^2)$. So CG method can be used as a reference solution for the analysis of the terrain profile.

In Chapter 4, Conjugate Gradient Method with Fast Fourier Transform is introduced and the acceleration of the approximated solutions are shown with same examples of terrain profiles chosen in this chapter. Also, the comparison of computational costs for the MoM solutions and the approximated CG-FFT solutions are tabulated in the next chapter.

Investigations on rough surface profiles show that CG method obtains numerically accurate results for both TM and TE polarization cases. CG reaches a residual error of 10^{-4} in less number of iterations for TE case

than TM case. For the last example, the numbers of required iterations are 458 and 138, respectively. But it's better not to use an upper limit for the number of iterations as a stopping criterion since this number is strongly dependent upon the number of unknowns to be solved. While direct inversion of MoM matrix method's computational cost is related to the matrix fill time and LU inversion, CG has a computational cost due to matrix-vector multiplication and number of iterations. Table 3.1 tabulates the computational cost of LU inversion of MoM and CG method for sea surface profile example.

Table 3.1: Computational cost for CG method

N	Matrix Fill (s)	LU inversion (s)	TM-CG (s)	TE-CG (s)
500	1.8	19.2	8.67	2.45
1000	9.2	172.5	42	11.6
2000	28.8	1705.67	169.34	55.2
3000	115	3455.5	384.6	102
4000	170	NA	752.6	234

From the table above, it is obvious that LU inversion requires $O\ (N^3)$ CPU-time while the CG requires $O\ (N^2)$ computational cost. The examinations and comparisons demonstrate that, the CG can be used as a reference solution instead of MoM for the study of scattering problems for both horizontal and vertical polarizations with a computational cost of $O\ (N^2)$. An interesting point is that the iteration number is reduced for imperfect conductor surface since the corresponding impedance matrices have better condition numbers.The authors of [37] and [38] agree with this result.

CHAPTER 4

CONJUGATE GRADIENT WITH FAST FOURIER TRANSFORM

4.1 Introduction

Direct methods for general matrix solution require the full $N \times N$ matrix to be stored in computer memory, placing a bottleneck on the solution process for large systems. If sufficient structure or sparsity is present in the equation of interest, iterative methods offer the possibility of avoiding this storage bottleneck. Iterative algorithms only require an implicit matrix operator (a subroutine that when given a column vector returns the product of the $N \times N$ system matrix with the column vector) and can easily exploit any type of matrix structure, [27].

4.2 Conjugate Gradient Method with Fast Fourier Transform

Electromagnetic problems posed in terms of integral equations with convolutional kernels can sometimes be discretized to yield matrices having discrete-convolutional symmetries. A general discrete convolution is an operation of the form, [22, 23],

$$e_m = \sum_{n=0}^{N-1} j_n g_{m-n} \tag{4.1}$$

where *e*, *j* and *g* denote sequences of numbers. (4.1) is equivalent to the matrix equation

$$\begin{bmatrix} g_0 & g_{-1} & g_{-2} & \cdots & g_{1-N} \\ g_1 & g_0 & g_{-1} & \ddots & \vdots \\ g_2 & g_1 & g_0 & \ddots & \vdots \\ \vdots & \ddots & \ddots & \ddots & \vdots \\ g_{N-1} & \cdots & \cdots & & g_0 \end{bmatrix} \begin{bmatrix} j_0 \\ j_1 \\ \vdots \\ \vdots \\ j_{N-1} \end{bmatrix} = \begin{bmatrix} e_0 \\ e_1 \\ \vdots \\ \vdots \\ e_{N-1} \end{bmatrix} . \qquad (4.2)$$

The $N \times N$ matrix depicted in (4.2) is a general *Toeplitz* matrix. All of the elements of this matrix are described by the $2N$ –1 entries of the first row and column, [27]. If the elements of the sequence g repeat with period N, so that

$$g_{n-N} = g_n \qquad n=1, 2, ..., N-1 \qquad (4.3)$$

the operation is known as a circular discrete convolution and the $N \times N$ matrix in (4.2) is circulant. Otherwise, the operation is a linear discrete convolution. Note that any linear discrete convolution of length N can be embedded into a circular discrete convolution of length $2N$–1. This can be accomplished by extending the original sequence g to repeat with period $2N$–1, zero padding the sequence j to length $2N$–1, and changing the upper limit of the summation in (4.1) to $2N$–2, [27].

The FFT algorithm is an efficient way of implementing the discrete Fourier transform, [22, 23],

$$\tilde{g}_n = \sum_{k=0}^{N-1} g_k e^{-j\frac{2\pi nk}{N}} \qquad n=0,1,...,N-1 \qquad (4.4)$$

The inverse discrete Fourier transform is defined as

$$g_k = \frac{1}{N} \sum_{k=0}^{N-1} \tilde{g}_n e^{j\frac{2\pi nk}{N}} \qquad k=0,1,...,N-1 \qquad (4.5)$$

For notational purposes,

$$\tilde{g} = \mathrm{FFT}_N(g) \qquad (4.6)$$

$$g = \mathrm{FFT}_N^{-1}(\tilde{g}) \qquad (4.7)$$

are used to denote the discrete Fourier transform pair for a sequence of length N. The discrete convolution theorem states that if (4.1) is a circular discrete convolution of length N, it is equivalent to

$$\tilde{e}_n = \tilde{j}_n \tilde{g}_n \qquad n=0,1,...,N-1 \tag{4.8}$$

If (4.1) is a linear discrete convolution, the equivalence holds if the linear convolution is embedded in a circular convolution of length $2N-1$ as described above.

To summarize, the discrete convolution operation of (4.1) is equivalent to a Toeplitz matrix multiplication. Furthermore, either can be implemented using the FFT and inverse FFT algorithm according to the discrete convolution theorem, [22, 23],

$$\boldsymbol{e} = \mathrm{FFT}_N^{-1}[\mathrm{FFT}_N(\boldsymbol{j})\mathrm{FFT}_N(\boldsymbol{g})] \tag{4.9}$$

If the discrete convolution is of the linear type, the FFTs must be of length $2N-1$ rather than length N. The above conclusions are easily generalized to two or three dimensions. The relationship established in (4.9) can be extended to multiple dimensions in an obvious manner, [27].

In this study, the bottleneck on the solution of the established system is the limited storage capacity of computers. The solution also takes longer time. As mentioned before, matrix filling and regular LU decompositon of MoM takes a very long time in $O(N^3)$ and the storage needed is in $O(N^2)$. The CG method reduces the solution time to $O(N^2)$ but the storage limitation still remains. The CG-FFT method described in previous pages is an appropriate solution for the MoM matrices arising in electromagnetics problems. Only a single row or a few rows may be enough to solve the system by CG-FFT. Next section includes

comparison of CG-FFT and MoM applications for the rough terrain and sea profiles sampled previously.

4.3 Numerical Results For Conjugate Gradient Method with Fast Fourier Transform (CG-FFT)

Operating frequency is chosen to be 10 GHz, which corresponds to a wavelength of 3 centimeters, for all of the results. Figure 4.1 illustrates a quasi-planar surface profile of length 200 λ. Surface impedance for imperfect conducting case is chosen to be $\eta_s = 25 + \mathrm{j}20$. Dipole antenna is located at 4.5 meters (150 λ) on the displacement axis 10 λ above the surface. Average radiated power is 25 Watts. Results are compared to those in Figure 3.11. As shown in Figure 4.1 (b) the induced current result due to TM polarized wave quite close to that obtained by MoM and the percentage error is given in Figure 4.1 (c) at every point to investigate coincidence. Percentage error is calculated by

$$\% \, \mathrm{e} = \frac{\mathrm{I}_{\mathrm{CG-FFT}} - \mathrm{I}_{\mathrm{MoM}}}{\mathrm{I}_{\mathrm{MoM}}} \times 100 \, . \qquad (4.10)$$

The next example uses a sea surface profile. Imperfect conducting case is considered in which the sea is assumed to have a surface impedance of $\eta_s = 76.4 - \mathrm{j}65.1$ and relative permitivity of sea is chosen as 78. Plane wave incidence is considered with an incidence angle of $\theta = \pi/30$.

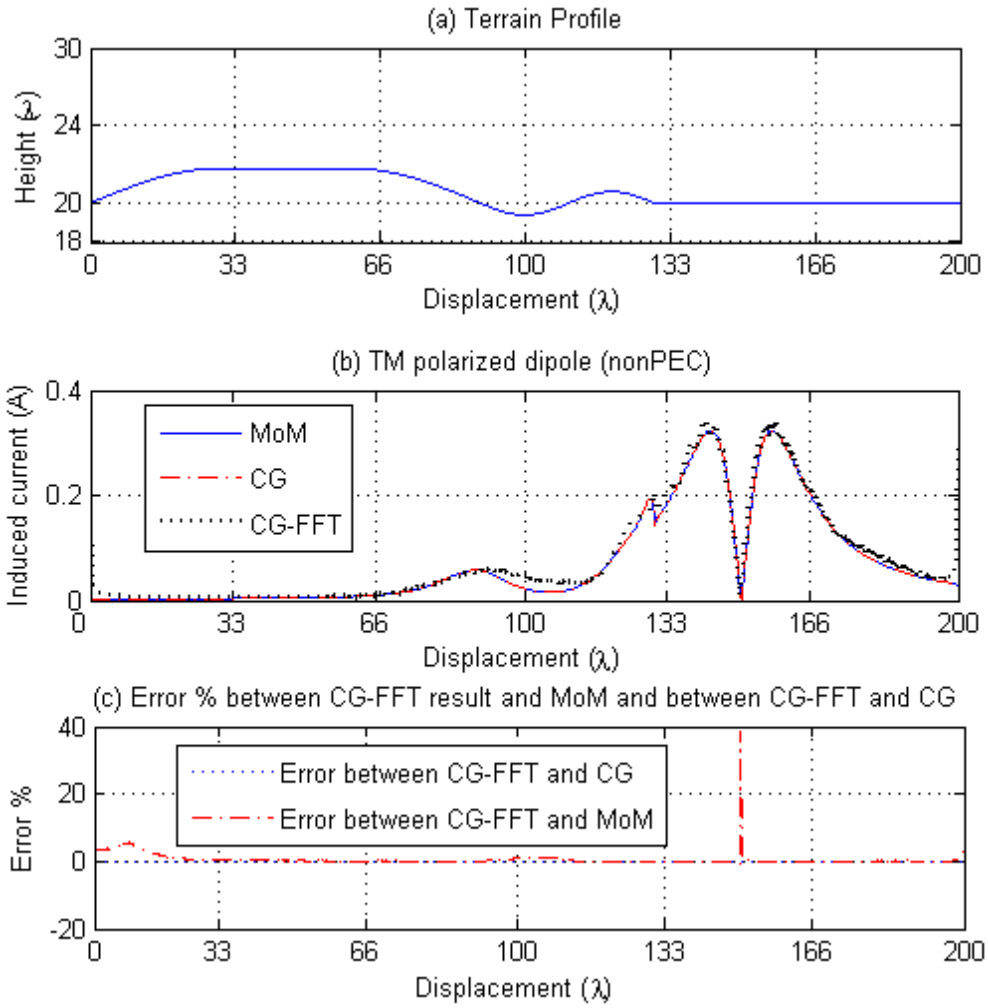

Figure 4.1: Dipole on a quasi-planar surface of width 200λ

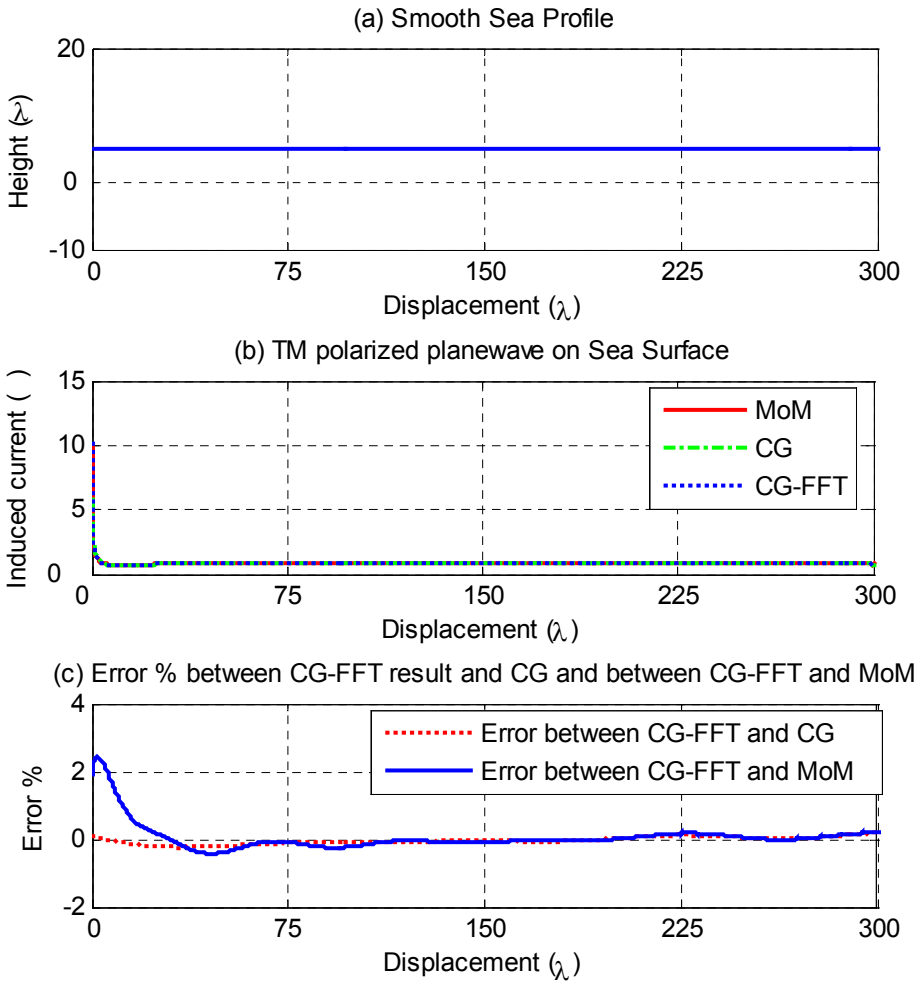

Figure 4.2: Distributed current on a 300λ rough surface, grazing plane wave

CHAPTER 5

ACCELERATED COMPUTATION OF FIELD STRENGTH ON ROUGH SURFACE PROFILES

5.1 Introduction

After the current distributions over the rough surface profile have been computed by the CG-FFT method, the next step is to compute the scattered field. If the region of interest corresponds to a small portion of the surface, the numerical evaluation of the total field will involve a reduced number of operations, but if these regions are extended to the complete terrain profile and the field strength is computed in a dense set of points, similar to the MoM discretization, the cpu-cost will increase up in $O(N^2)$, since the scattered field is expressed as,

$$E_y^{scat} \cong -\frac{\omega\mu}{4}\sum_{m=1}^{N} I_m \Delta x_m H_0^{(2)}\left(k\left|\rho_n - \rho_m\right|\right) - j\frac{k\eta_m}{4}\sum_{m=1}^{N} I_m \Delta x_m H_1^{(2)}\left(k\left|\rho_n - \rho_m\right|\right)\hat{n}_m \cdot \hat{\rho}_{nm} \tag{5.1}$$

and

$$H_y^{scat} \cong \frac{\omega \in \eta_m}{4}\sum_{m=1}^{N} I_m \Delta x_m H_0^{(2)}\left(k\left|\rho_n - \rho_m\right|\right) + j\frac{k}{4}\sum_{m=1}^{N} I_m \Delta x_m H_1^{(2)}\left(k\left|\rho_n - \rho_m\right|\right)\hat{n}_m \cdot \hat{\rho}_{nm} \tag{5.2}$$

for TM and TE polarization cases, respectively, [27]. Here I_m denotes the computed induced current on the source point ρ_n, and ρ_m denotes the observation point on which the scattered field will be obtained.

This $O(N^2)$ cost can make the method unsuitable for large terrain profiles. To overcome this limitation, acceleration with FFT can be applied in a similar way to compute the scattered field only with an $O(N\log N)$ cost. Equation (5.1) and (5.2) can be written as a matrix-vector multiplication. The CG-FFT can be employed for matrix-vector multiplications in which the impedance matrix is in Toeplitz form. The impedance matrix has a Toeplitz form for terrain profiles with small deviation.

Total field at any point over terrain profile can be found by

$$\begin{aligned} E_y^{tot} &= E_y^{scat} + E_y^{inc} \\ H_y^{tot} &= H_y^{scat} + H_y^{inc} \end{aligned} \tag{5.3}$$

5.2 Comparisons of Propagation Models with CGFFT Numerical Results

As a first example, the frequency is selected not in the x-band, but chosen as 1 GHz to investigate the accuracy of the method. The terrain profile used for this example is illustrated in Figure 5.1. An isotropic radiator is located at 60 meters for 300 meters terrain profile with 16 meters maximum deviation as shown in the figure. The free space model result is also shown in the figure for comparison. It can be seen that the free space model calculation has similarities to the CG-FFT result. The result of free space correction with Hata model, [46], is also shown in the figure. The computational cost of CG-FFT for Figure 5.1 with different deviations is illustrated in Table 5.1.

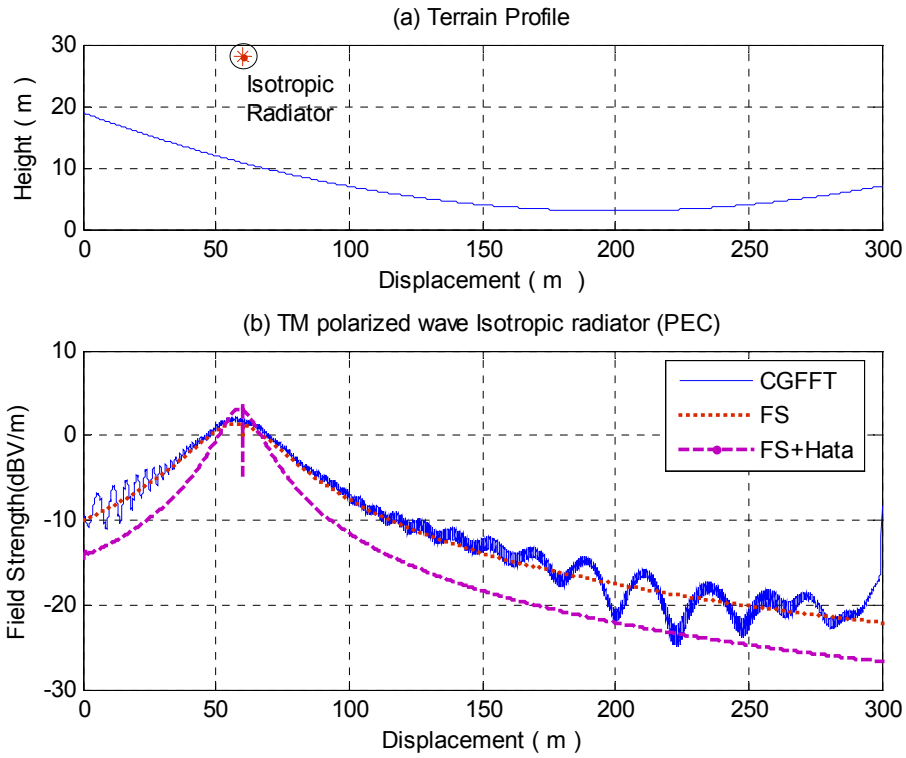

Figure 5.1: Field strength on a 300 m rough surface, with isotropic radiator at 1 GHz.

Table 5.1: Computational cost in MATLAB of CGFFT for Figure 5.1

N	Frequency	Deviation h/L	First Row Fill (s)	Induced Cur. with CGFFT(s)	Iteration number	Field Strength with CGFFT(s)
10000	1 GHz	0.01	0.545	1203	3854	2.4
10000	1 GHz	0.02	0.56	833	2540	2.5
10000	1 GHz	0.03	0.525	557	1636	2.6
10000	1 GHz	0.04	0.576	111.3	333	2.9
10000	1 GHz	0.05	0.544	235	687	2.24

Table 5.1 shows that if h/L is below 0.04, the number of iterations becomes higher due to worse conditioning of the impedance matrix. But if h/L is above 0.05 the Toeplitz form is broken down. So the method is limited to deviation of height.

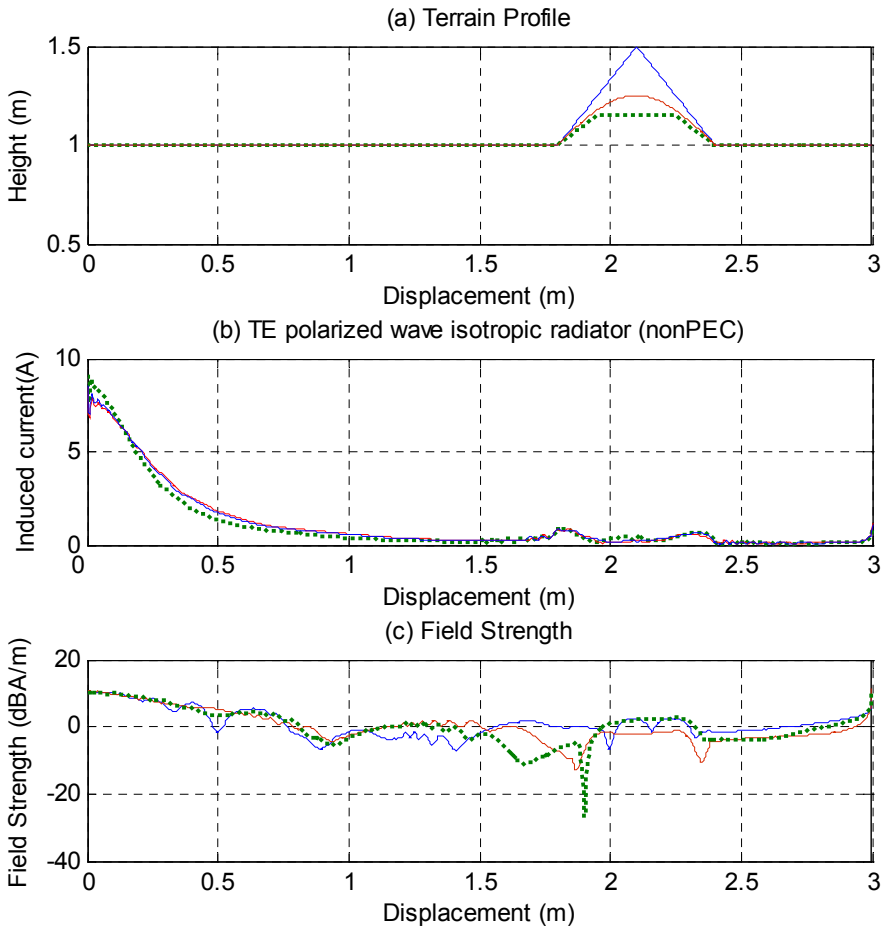

Figure 5.2: Field strength on a 3m multivalued rough surface with different roundnesses

Next example is shown in Figure 5.2. Now, the frequency is 10 GHz and the terrain has a length of 1000 λ, namely 3 m. An isotropic radiator is located at the left most of area, 30 centimeters above the

terrain. TE polarized wave is used. The area has two different regions: between 600 λ and 800 λ there is a PEC surface with 3 different roundness to investigate the diffraction, rest of the profile is modeled as smooth water region. Relative permittivity of sea water is 81 and surface impedance is $\eta_s = 76.4 - j65.1$. This example shows that the propagation over multivalued terrain profiles can be modelled. The results with CG-FFT is compared to Free Space model and is also compared to Free Space model recovered by paying attention to ground reflection, [47,48].

Another example is shown in Figure 5.3. Now, the frequency is 10 GHz and the terrain has a width of 10000 λ (N=100000), namely 300 m again. A dipole antenna is located at the left most of area. But this time, TE polarized wave is used. The terrain has different regions near the left most of Figure 5.3 (a), the needles symbolize two pines which model a knife-edge and near at right most there is a cottage with timber woods and the rest of area is modeled as sand. Relative permittivities of pines, timber woods, sand are 7, 2.5 and 5, respectively, and surface impedances of them are 109, 10^{12} and 10^{15}, respectively. This example shows that the propagation over multivalued terrain profiles can be accurately modeled. The results from CG-FFT is compared to both Free Space model and to Free Space model recovered by paying attention to knife-edge diffraction and ground reflection (indicated as RMD), [47,48].

Figure 5.1, Figure 5.2 and Figure 5.3 shows that the CG-FFT method gives reliable results with some limitations. Limitations are covered in the last chapter.

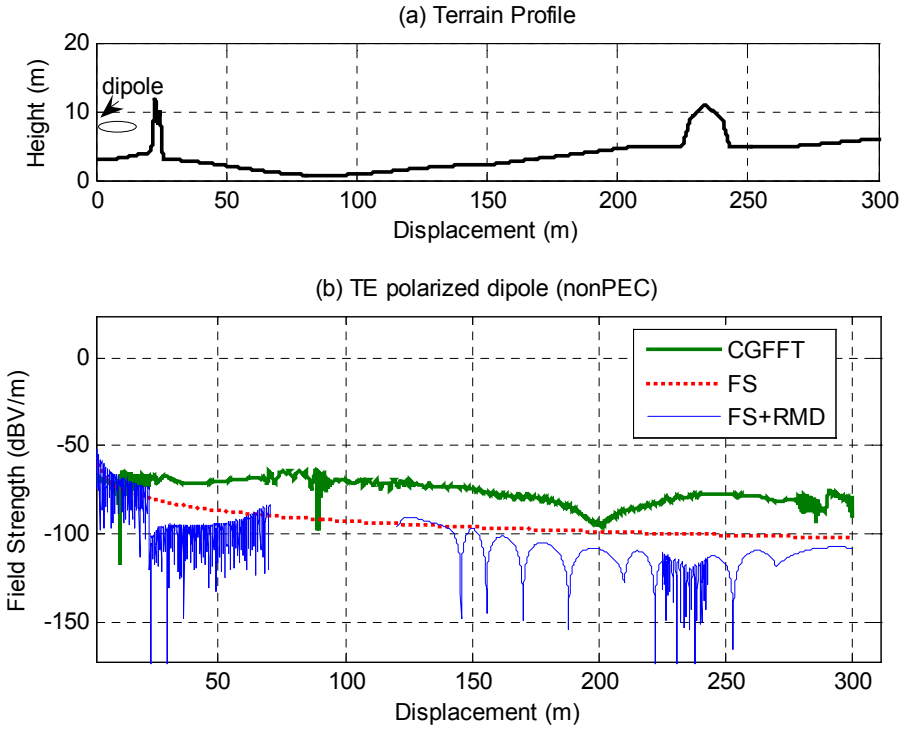

Figure 5.3: Field strength on a 300 m rough surface, with dipole antenna at 10 GHz.

CHAPTER 6

CONCLUSION

In this thesis, conventional CG and CG-FFT methods over various kinds of terrain profiles rough in one dimension and multi valued surfaces have been implemented by examples.

In order to compare the accuracy of CG method, results have been tested with reference direct inversion of MoM matrix solutions for both TM and TE polarization cases up to N = 3000 unknowns. This limitation is due to storage requirement to keep interaction matrices of MoM and due to computational cost of the direct solution technique, LU inverison which has an operation count of $O(N^3)$.

Numerical examples have shown that CG methods yield precise current distributions with a computational cost of $O(N^2)$ per iteration. An interesting result is that in the solution of induced current arising from TE polarized wave incidence on non-PEC surfaces, the iteration number is reduced for imperfect conductor surface due to the better conditioning of impedance matrices.

Later on, accelerated CG method has been applied over slightly rough surfaces with different height deviations. By this method, only a few rows of impedance matrice are used because the impedance matrice is diagonally dominant for quasiplanar surfaces. Results of CG-FFT method with respect to MoM and CG method have been investigated.

Numerical results for quasi-planar surfaces have shown that FFT algorithm works properly with CG. Error percentages of induced currents are very small for smaller height changes to the distance. This situation also confirms that the CG-FFT method works very well for Toeplitz form matrices. If one makes the impedance matrice in form of Toeplitz, it is sure that the CG-FFT works properly. Another result accompanied this result; the solutions for undulating geometries by CG-FFT method are not tolerable. Approximation works only for small height changes on the terrain and sea surfaces with very small wind effect.

The main product of this work is to present electrically large rough surface scattering analysis with CG-FFT method up to very large unknowns. Another innovation is the examination of multi-valued surface profiles without any computational complexity or high memory requirements. Based on these results, it can be used with general scattering problems confidentially.

There are also some limitations of the method. The major limitation in this method is that the matrix must be in Toeplitz form. In this thesis, it is provided by some interpolation and extrapolation algorithms on functional space and it is also provided by making height changes on the terrain profile small compared to displacement. That is, the MoM points over surface line are redistiributed by interpolation and the matrix becomes more closer to Toeplitz form. Although there are some methods employing non-uniform FFT in the literature, they are not considered in this thesis. By small deviation in terrain samples, the CG-FFT method on these is usable. This is the great limitation of the method in the thesis. And there is another limitation arising from

height-displacement relation with an oppurtunity cost between better-conditioning impedance matrix and Toeplitz form matrix.

Future work will focus on accelerating CPU processing time of the CG-FFT method. Since it depends on matrix – vector multiplies, it is well suited to parallel processing. Furthermore, some modifications corresponding to the acceleration algorithm may be implemented to analyze undulating terrain profiles in the rural and urban areas and also using non-uniform FFT can be considered which does not require interpolation to put the impedance matrices into Toeplitz form. In this respect Fast Multipole Method will also be useful.

REFERENCES

[1] "Special issue on low-grazing-angle backscattering from rough surfaces", IEEE Trans. Antennas and Propagat., vol. 46, Jan. 1998.

[2] R.F. Harrington, Field Computation by Moment Method, IEEE Press, 1993.

[3] "VHF and UHF propagation curves for the frequency range from 30 MHz to 1000 MHz", Recommendation ITU-R P.370-7, 1995.

[4] "Prediction methods for the terrestrial land mobile service in the VHF and UHF bands", Recommendation ITU-R P.529-3, 1999.

[5] "Method for point-to-area predictions for terrestrial services in the frequency range 30 MHz to 3000 MHz", Recommendation ITU-R P.1546, 2001.

[6] "Federal Communications Commission Curves", www.fcc.gov. Last accessed date: 22.7.2007.

[7] C.L. Rino and H.D. Ngo, "Forward propagation in half-space with an irregular boundary", IEEE Trans. Antennas and Propagat., vol. 45, pp. 1340-1347, Sept. 1997.

[8] D.J. Donohue and J.R. Kuttler, "Propagation modeling over terrain using the parabolic wave equation", IEEE Trans. Antennas and Propagat., vol. 48, pp. 260-277, Feb. 2000.

[9] A.E. Barrios, “A terrain parabolic equation model for propagation in the troposphere”, IEEE Trans. Antennas and Propagat., vol. 42, pp. 90-98, Jan. 1994.

[10] L.Sevgi, “Elektromanyetik Problemler ve Sayısal Yöntemler”, Birsen Yayınevi, 1999

[11] S. Ayasli ”SEKE: A computer model for low altitude radar propagation over irregular terrain”, IEEE Trans. Antennas and Propagat., vol. AP-34, pp. 1013-1023, Aug. 1986.

[12] R.J. Luebbers, “Finite conductivity uniform GTD versus knife edge diffraction in prediction of propagation path loss”, IEEE Trans. Antennas and Propagat., vol. AP-32, pp. 70-76, Jan. 1984.

[13] R. Janaswamy, “A Fredholm integral equation method for propagation over small terrain irregularities”, IEEE Trans. Antennas and Propagat., vol. 40, pp. 1416-1422, Sept. 1994.

[14] J.T. Hviid, J.B. Anderson, J. Toftgard, and J. Bojer, “Terrain based propagation model for rural area - an integral equations approach”, IEEE Trans. Antennas and Propagat., vol. 43, pp. 41-46, Jan. 1995.

[15] D. Holliday, L.L. DeRaad Jr., and G.J. St.-Cyr, “Forward-Backward: A new method for computing low-grazing scattering”, IEEE Trans. Antennas and Propagat., vol. 44, pp. 722-729, May 1996.

[16] R. Barret, M. Berry, T.F. Chan, J. Demmel, J. Donato, J. Dongarra, V. Eijkhout, R. Poza, C. Romine, and H.Ban der Vort, “Templates for the Solution of Linear Systems: Building Blocks for Iterative Methods”, SIAM, 1994.

[17] C.F. Smith, A. F. Peterson, and R. Mittra, “The biconjugate Gradient Method for electromagnetic scattering”, IEEE Trans. Antennas and Propagat., vol. 38, pp. 938-940, June 1990.

[18] P. Cao and C. Macaskill, “Iterative techniques for rough surface scattering problems”, Wave Motion, vol. 21, pp. 209-229, 1995.

[19] D.J. Donohue, H.C. Ku, and D.R. Thompson, “Application of iterative moment-method solutions to ocean surface radar scattering”, IEEE Trans. Antennas and Propagat., vol. 46, pp.121-132, Jan. 1998.

[20] F. Chen, “The numerical calculation of two-dimensional rough surface scattering by the conjugate gradient method”, Int. J. Remote Sensing, vol. 17, no. 4, pp. 801-808, 1996.

[21] H.T. Chou and J.T. Johnson, “A novel acceleration for the computation of scattering from rough surfaces with the forward-backward method”, Radio Sci., vol. 33, pp. 1277-1287, Jun. 1998.

[22] E.O. Brigham, “The fast fourier transform”, Prentice Hall,1974.

[23] A.V. Oppenheim and R.W. Schafer, “Digital Signal Processing”, Englewood Cliffs, NJ: Prentice Hall,1975.

[24] C.C. Su, “Calculation of electromagnetic scattering from a dielectric cylinder using the conjugate gradient method and FFT”, IEEE Trans. Antennas and Propagat., vol. AP-35, pp.1418-1425, Dec. 1987.

[25] T.J. Peters and J.L. Volakis, “Appliation of a conjugate gradient FFT method to scattering from thin material plates”, IEEE Trans. Antennas and Propagat., vol. AP-36, pp.518-526, Apr. 1988.

[26] D.T. Borup and O.P. Gandhi, “Calculation of high resolution SAR distribution in biological bodies using the FFT algorithm and conjugate gradient method”, IEEE Trans. Microwave Theory Tech., vol. MTT-33, pp.417-419, May 1985.

[27] A.F. Peterson, S.L. Ray and R. Mittra, “Computational methods for electromagnetics”, IEEE Press Series on Electromagnetic Waves, IEEE Press, 1997.

[28] T.K. Sarkar, ed., “Application of conjugate gradient method to electromagnetics and signal analysis”, NY: Elsevier, 1991

[29] V. Rokhlin, “Rapid solution of integral equations of classical potential theory”, J. Computat. Phys., vol. 60, pp.187-207, 1985

[30] C.C. Lu and W.C. Chew, “Fast algorithm for solving hybrid integral equations“, IEE Proc. Part H, vol. 140, no.6, pp. 455-460, Dec. 1993.

[31] L.N. Medgyesi-Mitschang, J.M. Putnam, “Integral Equation Formulations for Imperfectly Conducting Scatterers”, IEEE Trans. Antennas and Propagat., vol. AP-33, no. 2, Feb. 1985.

[32] R.D. Graglia and P.L.E. Uslenghi, “Electromagnetic scattering by impedance bodies of revolution”, Nat. Radio Sci. Meeting, session URSI/B-6-3, paper 4, Univ. Houston, Houston, TX, 23-26 May 1983.

[33] T. B. A. Senior, “Impedance boundary conditions for imperfectly conducting surfaces”, Appl. Sci. Res., vol. 8, pp. 418-436, 1961.

[34] K. M. Mitzner, “An integral equation approach to scattering from a body of finite conductivity”, Radio Sci. Res., vol. 2, 1967.

[35] D.-S. Wang, “Limits and validity of the impedance boudary condition on penetrable surfaces”, IEEE Trans. Antennas and Propagat., vol. AP-35, Apr. 1987.

[36] S.-W. Lee and W. Gee, ”How good is the impedance boundary condition?”, IEEE Trans. Antennas and Propagat., vol. 50, Nov. 1987.

[37] Barış Babaoğlu, “Application of biconjugate gradient stabilized method with spectral acceleration for propagation over terrain profiles”, M.Sc. Thesis, Bilkent University, 2003

[38] Celal Alp Tunç, “Application of spectral acceleration forward-backward method for propagation over terrain”, M.Sc. Thesis, Bilkent University, 2003

[39] R. Mittra and A. Peterson, “Numerical techniques for RCS computation and scattering center approach to RCS modeling”, Lecture Note, vol. 2

[40] E. A. Ericson and D. R. Lyzenga, “Performance of a numerical iterative solution of the surface current integral equation for surfaces containing small radii of curvature”, Radio Sci., vol.33, 1998

[41] D. A. Kapp and G. S. Brown, “A new numerical-method for rough surface scattering calculations”, IEEE Trans. Antennas and Propagat., vol. 44, May 1996.

[42] A. F. Peterson, S. L. Ray, C. H. Chan and R. Mittra, “ Numerical implementation of the conjugate gradient method and the CG-FFT for electromagnetic scattering”, Application of Conjugate Gradient Method to Electromagnetics and Signal Analysis, ed. T.K. Sarkar, Elsevier, 1991

[43] M. R. Hestenes and E. Steifel, “Methods of conjugate gradients for solving linear systems”, J. Res. Nat. Bur. Stand., vol. 49, 1952

[44] S. F. Ashby, T. A. Manteuffel and P. E. Saylor, “A taxonomy for conjugate gradient methods”, Dept. of Comp. Science Rep. UIUC-DCS-R-88-1414, Univ. of Illinois, Urbana, April, 1988

[45] J. Stoer, “Solution of large linear systems of equations by conjugate gradient type methods”, Mathematical Programming: The State of Art, eds. A. Bachem, M. Grötschel and B. Korte, Springer, New York, 1983.

[46] M. Hata, “Empirical formula for propagation loss in land mobile radio services”, IEEE Trans.Vehicular Tech., vol. VT-29, no. 3, August 1980.

[47] J. Deygout, “Multiple knife-edge diffraction of microwaves”, IEEE Trans. Antennas and Propagat., vol. 14,1966.

[48] B. Beckmann and A. Spizzichino, “The scattering of electromagnetic waves from rough surfaces”, MacMillan, 1963.